Large Aperture X-ray Monitors for Beam Profile Diagnostics

Cyrille Thomas
Guenther Rehm
Frederike Ewald
John Flanagan

Content

- Source
  - Emittance, Storage rings, Ultimate Storage Rings
  - Photon beam: Bending Magnet, Undulators
- Image
  - Large Aperture definition
    - Coherent and incoherent imaging
    - Resolution, Deconvolution techniques, etc.
- Coded Apertures
  - URA, MURA, etc, masks
  - Zone Plates
- CRL
- Comparison with other profile measurement systems
- Conclusion

Source

- Emittance, Storage rings, Ultimate Storage Rings
  - Emittance trend reduces over the SR generations,...

Source

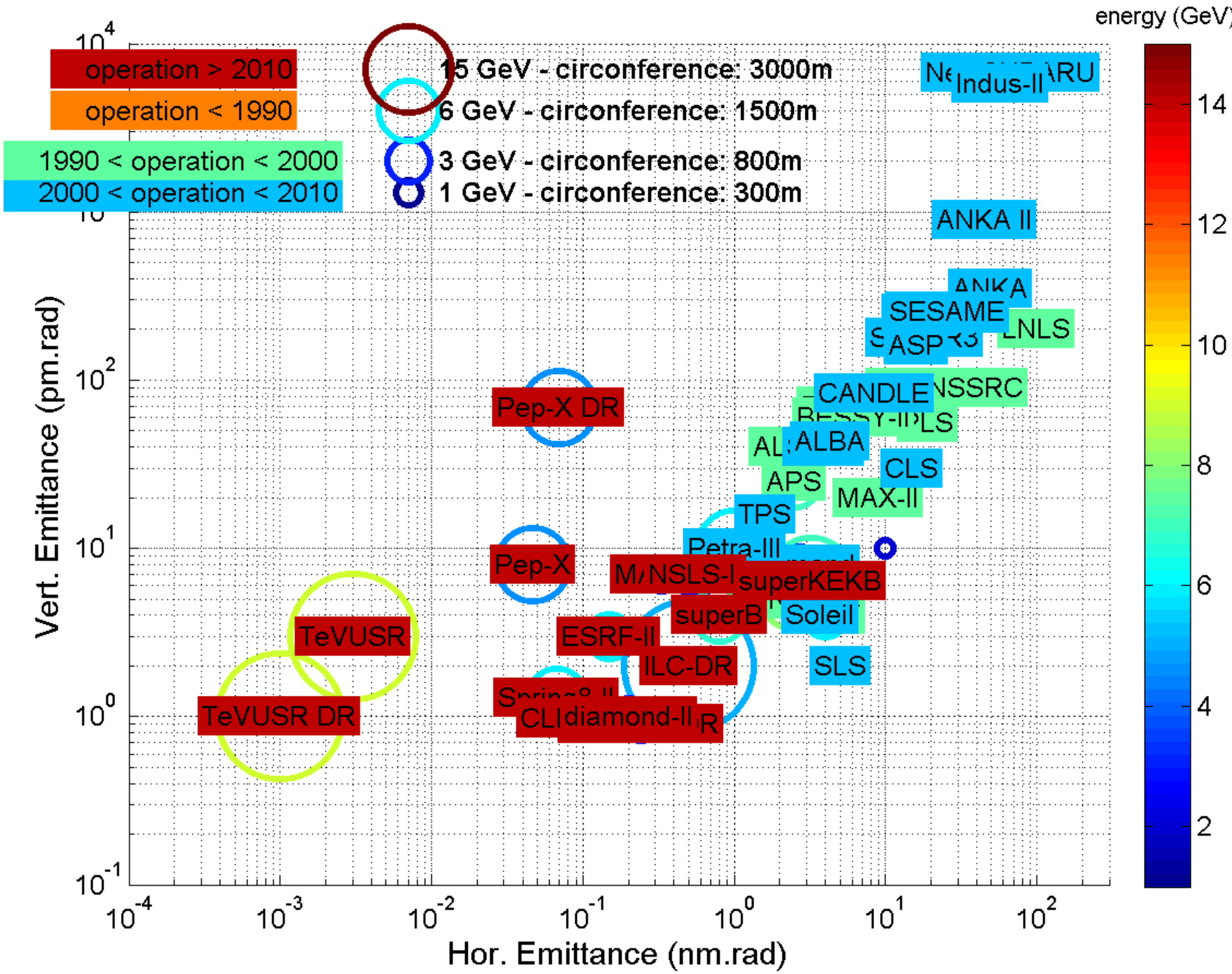
operation > 2010
operation < 1990
1990 < operation < 2000
2000 < operation < 2010
15 GeV - circonference: 3000m
6 GeV - circonference: 1500m
3 GeV - circonference: 800m
1 GeV - circonference: 300m
energy (GeV)
14
12
10
8
6
4
2
Indus-II
ANKA II
SESAME
ASP
CANDLE
ALBA
CLS
APS
MAX-II
TPS
Petra-III
superKEKB
superB
Soleil
SLS
ESRF-II
ILC-DR
diamond-II
Pep-X DR
Pep-X
TeVUSR
TeVUSR DR
Vert. Emittance (pm.rad)
Hor. Emittance (nm.rad)

Source

- Emittance, Storage rings, Ultimate Storage Rings
  - Emittance trend reduces over the SR generations, and so the beam size

Source

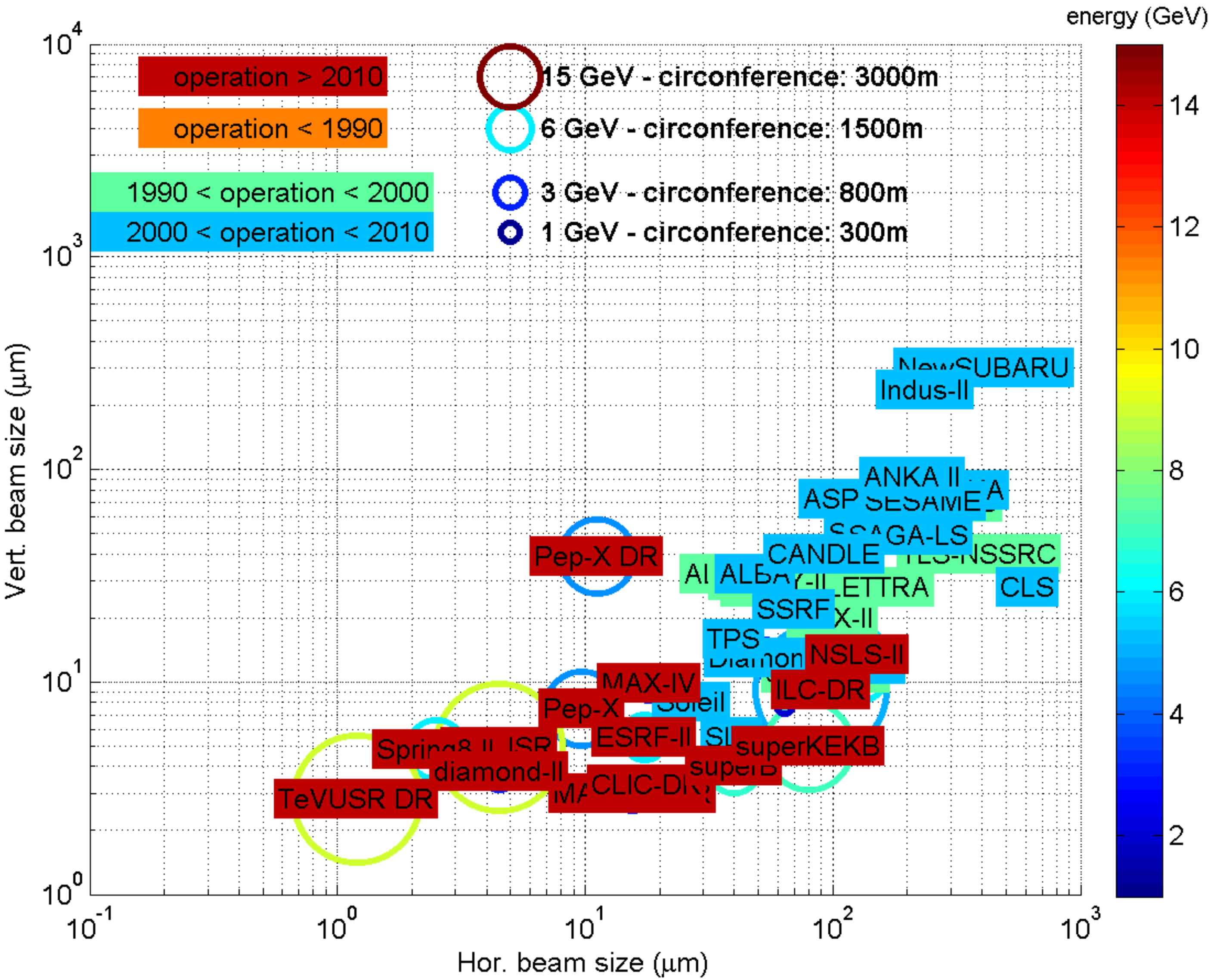
operation > 2010
operation < 1990
1990 < operation < 2000
2000 < operation < 2010
15 GeV - circonference: 3000m
6 GeV - circonference: 1500m
3 GeV - circonference: 800m
1 GeV - circonference: 300m
energy (GeV)
Vert. beam size (μm)
Hor. beam size (μm)
Indus-II
ANKA II
ASP
CANDLE
CLS
SSRF
TPS
NSLS-II
ILC-DR
MAX-IV
Pep-X DR
Pep-X
ESRF-II
superKEKB
diamond-II
TeVUSR DR

Source

- Bending Magnet source properties
  - Quasi-homogeneous X-ray source
  - Non-stationary (pulsed)

- Known solution of the source expression and of the spectral degree of coherence
- Behaves like a laser beam in vertical plane and like a infinite diverging source in the horizontal plane
- For X-ray beam, photon beam emittance much larger than the wavelength: geometrical optics approach can be used

Geloni *et al*, Statistical Optics approach to the design of beamlines for Synchrotron Radiation arXiv:physics/0603269

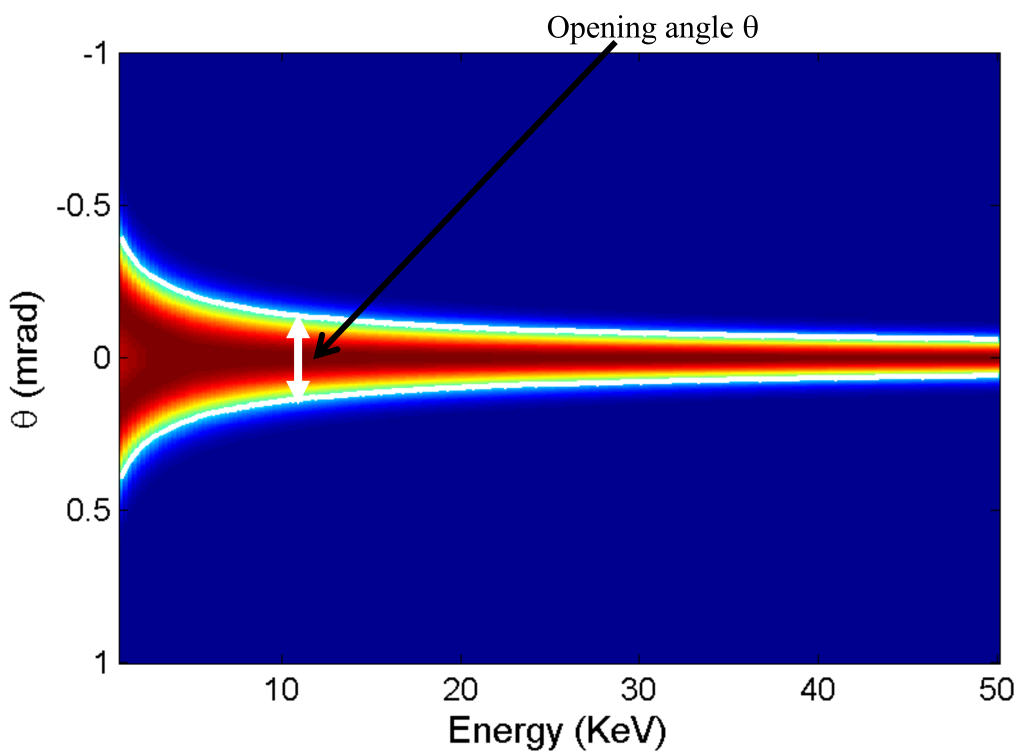

- Undulator Source properties
  - Quasi-homogeneous source (incoherent) provided

$$\hat{N} = \frac{\sigma_{x,y}^2\,\omega}{c\,L_w} \gg 1 \text{ and } \hat{D} = \frac{\sigma_{x',y'}^2\,\omega\,L_w}{c} \gg 1$$

  - Non-homogeneous source (partially coherent)

$$\hat{N} = \frac{\sigma_{x,y}^2\,\omega}{c\,L_w} \simeq 1 \text{ and } \hat{D} = \frac{\sigma_{x',y'}^2\,\omega\,L_w}{c} \simeq 1$$

  - Non-homogeneous source (coherent)

$$\hat{N} = \frac{\sigma_{x,y}^2\,\omega}{c\,L_w} \ll 1 \text{ and } \hat{D} = \frac{\sigma_{x',y'}^2\,\omega\,L_w}{c} \ll 1$$

  - Non-stationary (pulsed)

Geloni *et al*, Statistical Optics approach to the design of beamlines for Synchrotron Radiation arXiv:physics/0603269

- Undulator Source properties
  - Intensity profile: laser beam like with opening angle: $\theta_{u,n} = \sqrt{\frac{\lambda_n}{2L_u}}$
  - Flux: $\frac{d\Phi_n}{d\Omega}_{[Photons/s/0.1\%/mrad^2]} = 1.744\,10^{14} N_w^2 E_{[GeV]}^2 I_{[A]} F_n(K)$
    - Diamond U23 with N=90, 3rd Harmonic at 10keV
      - $\Phi_n \approx 10^{18}$ Photons/s/0.1%bw
      - $\theta_{u,3} \approx 5$ µrad

Source

- Large Aperture definition
  - Imaging device that has a numerical aperture comparable or larger than the X-ray beam numerical aperture

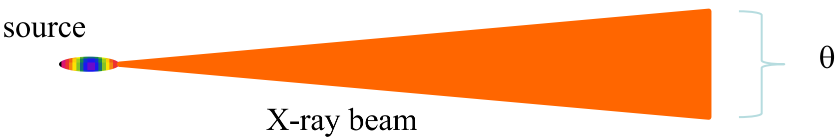

Numerical Aperture:
NA = sin(θ)

Resolution:
R = λ / 2 NA

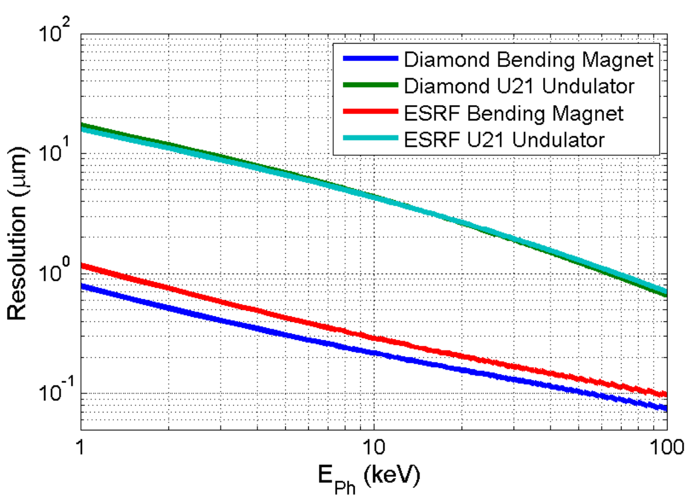

Source	NA @ 10 keV	Resolution (µm) @ 10 keV	Aperture (mm) @ D = 10 m
U21 undulator (Diamond)	1.4×10^{-5}	4.2	0.14
U21 undulator (ESRF)	1.4×10^{-5}	4.2	0.14
Bending Magnet (Diamond)	2.8×10^{-4}	0.2	2.8
Bending Magnet (ESRF)	2.2×10^{-4}	0.3	2.2

Image

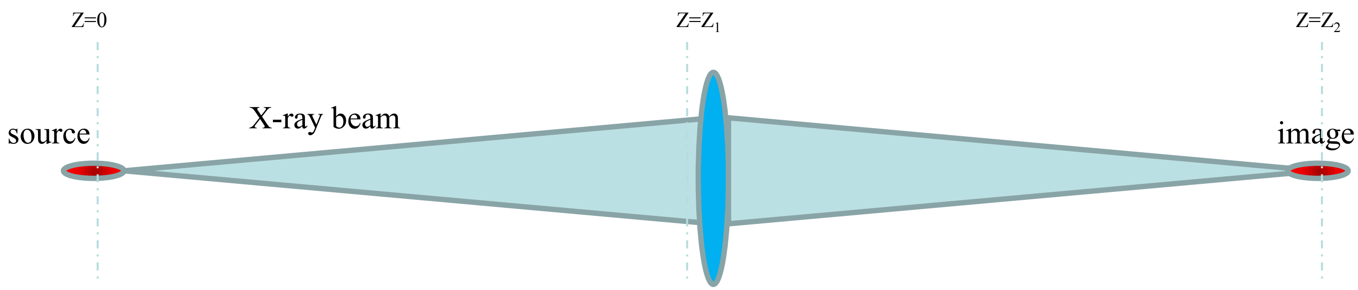

$$\vec{E}\,(t,\omega,Z=0)$$
$$\Gamma\left(\omega,\vec{X},Z=0\right)$$

$$\vec{E}_i\,(t,\omega,Z=0)$$
$$\Gamma_i\left(\omega,\vec{X},Z=Z_1\right)$$

Image: 2D Fourier Transform, scaled source

$$I(x,y)=\frac{1}{(\lambda z)^2}\int_{-\infty}^{-\infty}\int_{-\infty}^{-\infty}\boxed{\widetilde{P}(\Delta\xi,\Delta\eta)}\,\boxed{\Gamma_i(\Delta\xi,\Delta\eta)}\,e^{i\frac{2\pi}{\lambda z}(x\Delta\xi+y\Delta\eta)}d\Delta\xi\,d\Delta\eta$$

Fourier transform of the pupil autocorrelation

$$\widetilde{P}(\Delta\xi,\Delta\eta)=\frac{1}{(\lambda z)^2}\int_{-\infty}^{-\infty}\int_{-\infty}^{-\infty}P(\bar{\xi}-\frac{\Delta\xi}{2},\bar{\eta}-\frac{\Delta\eta}{2})\,P^*(\bar{\xi}+\frac{\Delta\xi}{2},\bar{\eta}+\frac{\Delta\eta}{2})\,e^{i\frac{2\pi}{\lambda z}(x\Delta\xi+y\Delta\eta)}d\Delta\xi\,d\Delta\eta$$

Γ_i Mutual Coherence in front of the lens

diamond

See Goodman, Statistical optics, ISBN 0-47 1-3991 6-7

Image: Incoherent imaging and Deconvolution

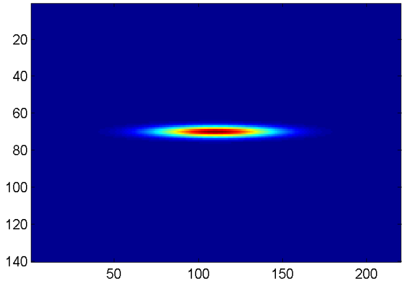

$\otimes$

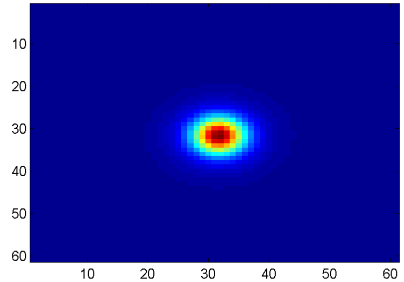

=

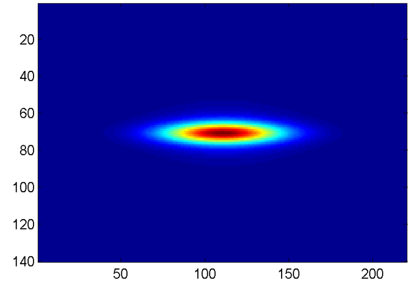

object

imaging system:
PSF

image

Inverse Fourier

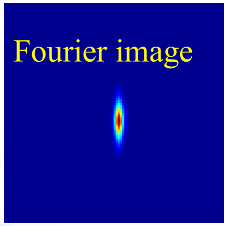

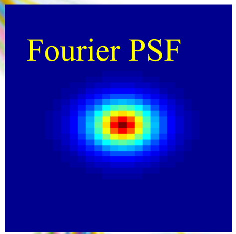

=

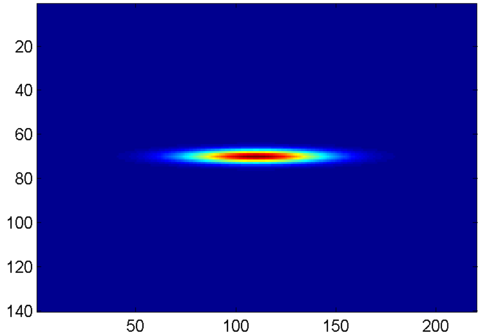

object

Deconvolution and Noise Limitation

- Major Problem: Noise in the image

$$g(x,y) = h(x,y) \otimes o(x,y) + n(x,y)$$

in the Fourier space:

$$G(\nu,\eta) = H(\nu,\eta)\ O(\nu,\eta) + N(\nu,\eta)$$

  - Solution: introduce a noise filter in the deconvolution algorithm
    - Example: Wiener filter:
      - » the algorithm seek an estimate o(x,y) that minimises the statistical error function $|g - F^{-1}(G./\ H + N)|^2$ and in which a low pass filter is introduced

  - Other solution: iterative nonlinear algorithm
    - Example Lucy-Richardson:
      - » based on maximum-likelihood formulation in which the image is modelled with Poisson statistics
      - » Rapid convergence to the real solution:
        - » G. Zech, doi http://dx.doi.org/10.1016/j.nima.2013.03.026

Deconvolved beam size with a range of defined apertures

- Vertical emittance $\varepsilon \approx 1.3$ pm.rad, $\sigma \approx 5.5$ µm

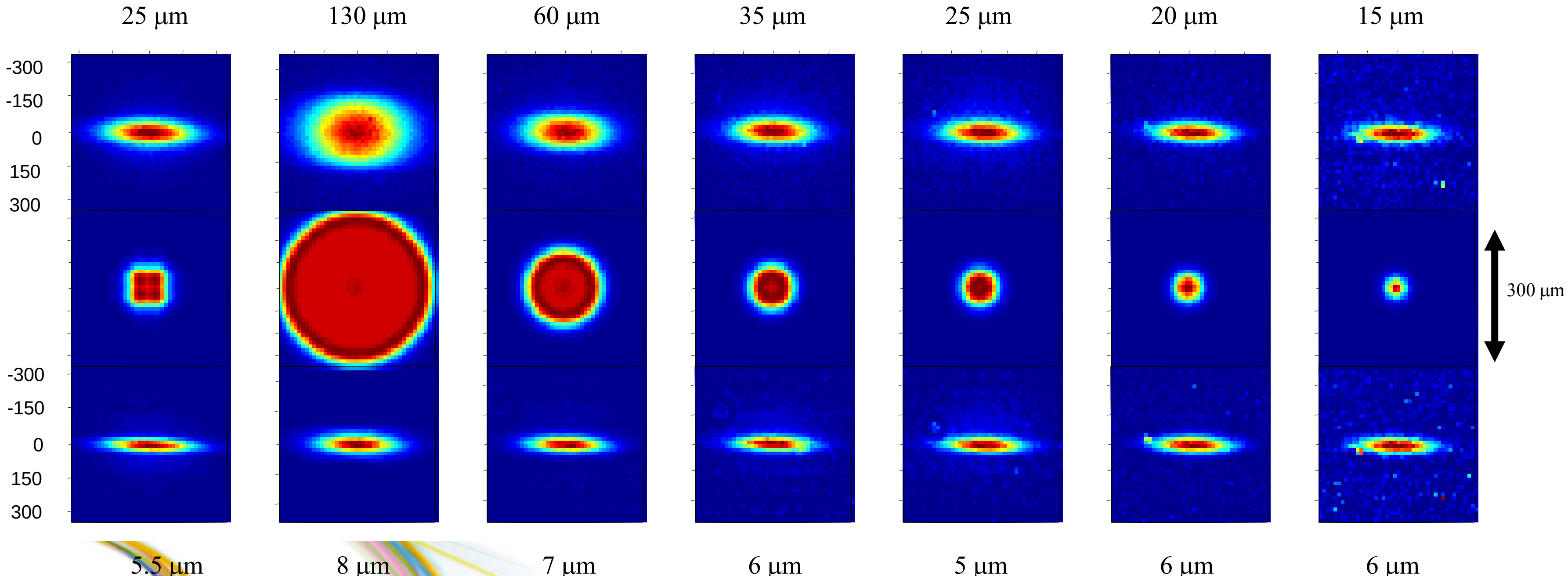

Thomas *et al.*, BIW 2012, TUA01

Coded Aperture and Pinhole Camera Imaging

Courtesy of A. Haboub

- Small pinhole allows little light ➔inefficient

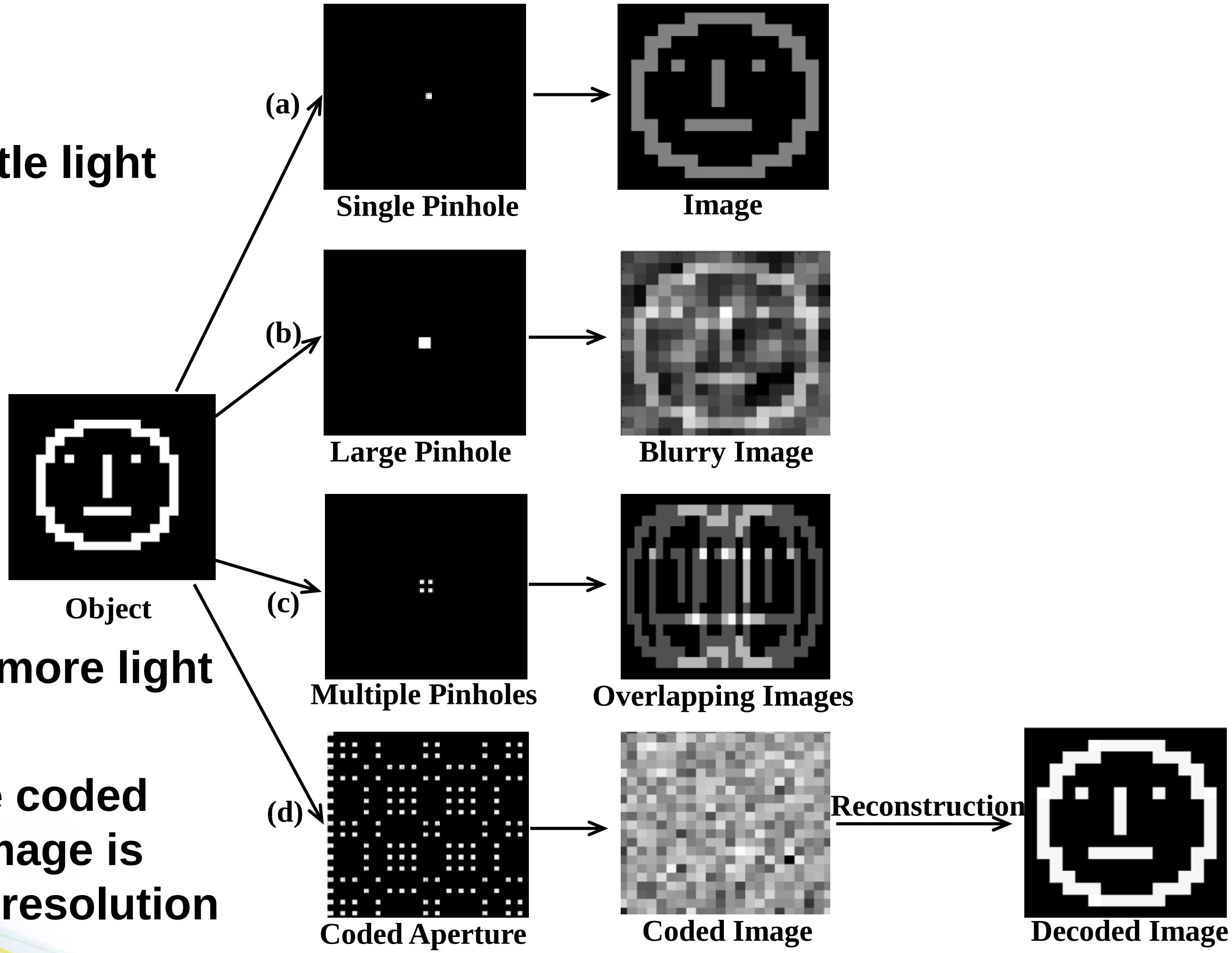

- Several pinholes allow more light ➔ overlapping images

By choosing a suitable coded aperture pattern the image is decoded with a better resolution

umerous Coded Aperture Patterns

Courtesy of A. Haboub

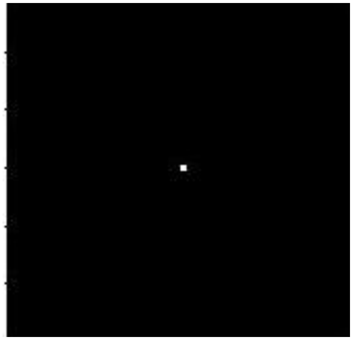

Pinhole

Fresnel Zone Plate (FZP)

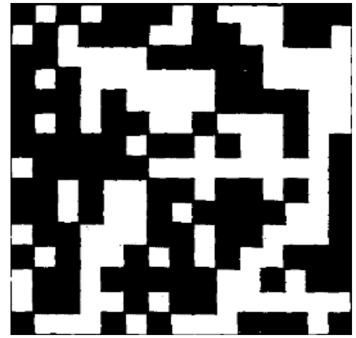

random mask

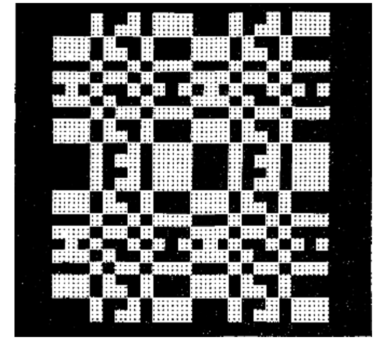

URA mask

MURA
50% open area

$\mathbf{A(i,j)}$

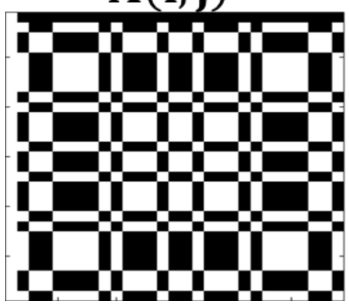

Modified Uniformly Redundant Array (MURA)

$$\mathbf{B = kron(A,h)}$$

$$\mathbf{h = zeros(2)}$$

$$\mathbf{h(1,1) = 1}$$

$\mathbf{B(i,j)}$

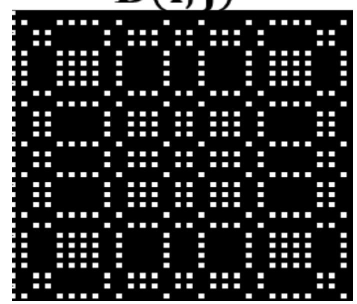

Non Two Holes Touching (NTHT)

NTHT MURA
0.4% open area

$\mathbf{A(i,j)}$

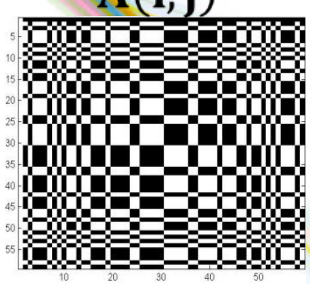

$\otimes$

$\mathbf{\tilde{A}(i,j}$

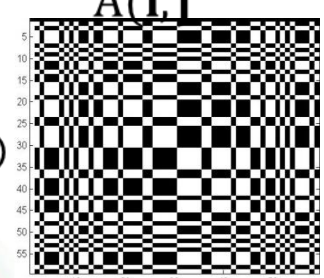

$=$

SPSF

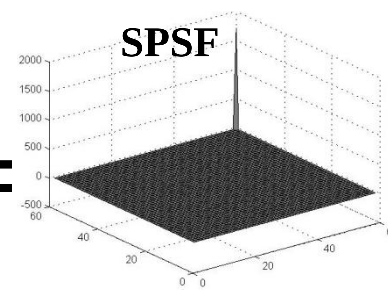

$$\mathbf{A(i,j) \otimes \tilde{A}(i,j) = \delta}$$

Coded aperture imaging simulation

Courtesy of A. Haboub

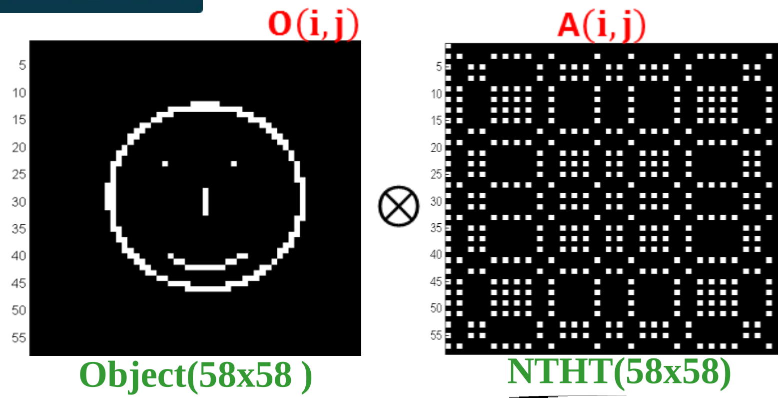

$$\mathbf{I(i,j) = O(i,j) \otimes A(i,j)} \quad \mathbf{(1)}$$

The detected flux at pixel j and k is:

$$\mathbf{I_{jk} = \sum_l \sum_k A_{j+l,k+i}\ O_{li}} \quad \mathbf{(2)}$$

By deriving $\tilde{A}$: $\mathbf{\tilde{A} = ifft2(1./fft2(A))}$ **(3)**

The reconstructed image O' is:

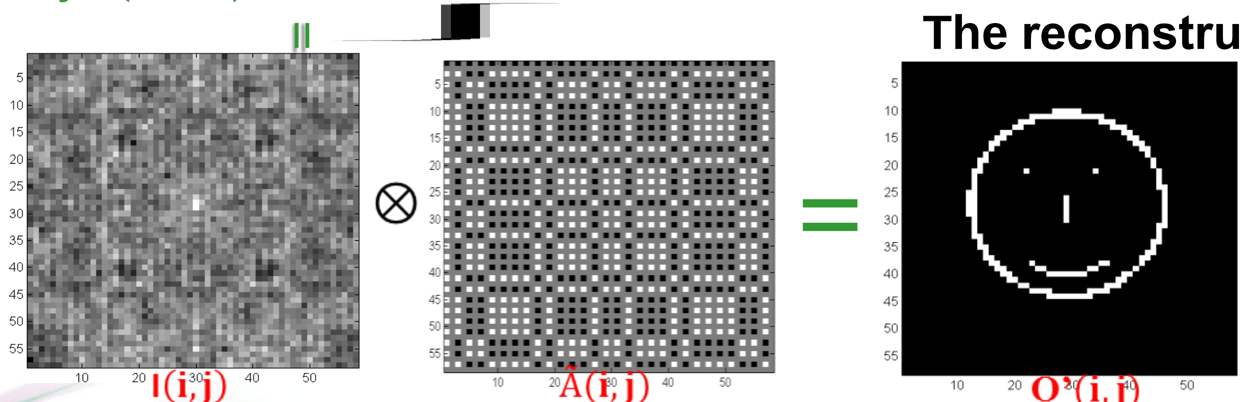

$$\mathbf{O'(i,j) = I(i,j) \otimes \tilde{A}(i,j)} \quad \mathbf{(3)}$$

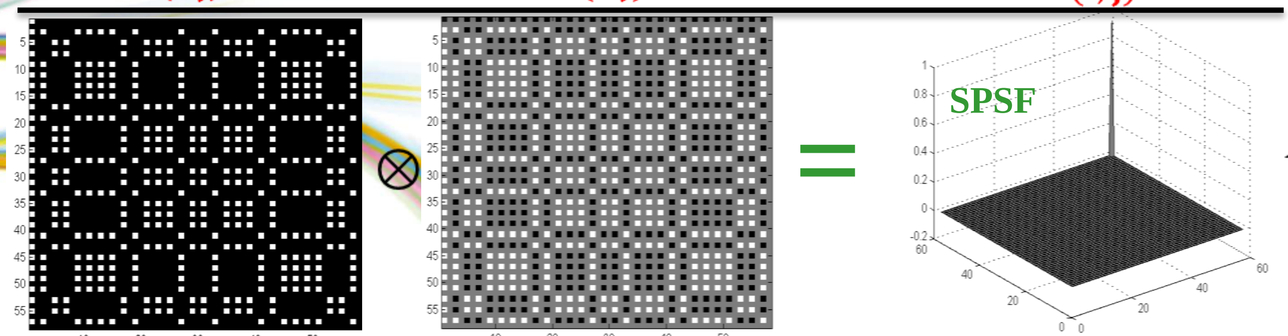

$$\mathbf{A(i,j) \otimes \tilde{A}(i,j) = \delta} \quad \mathbf{(4)}$$

For cosmic rays, Coded aperture imaging using NTHT works with simple convolution because the coded image and NTHT pattern has the same size.

Simulation of the image reconstruction from Coded Aperture Imaging

Courtesy of A. Haboub

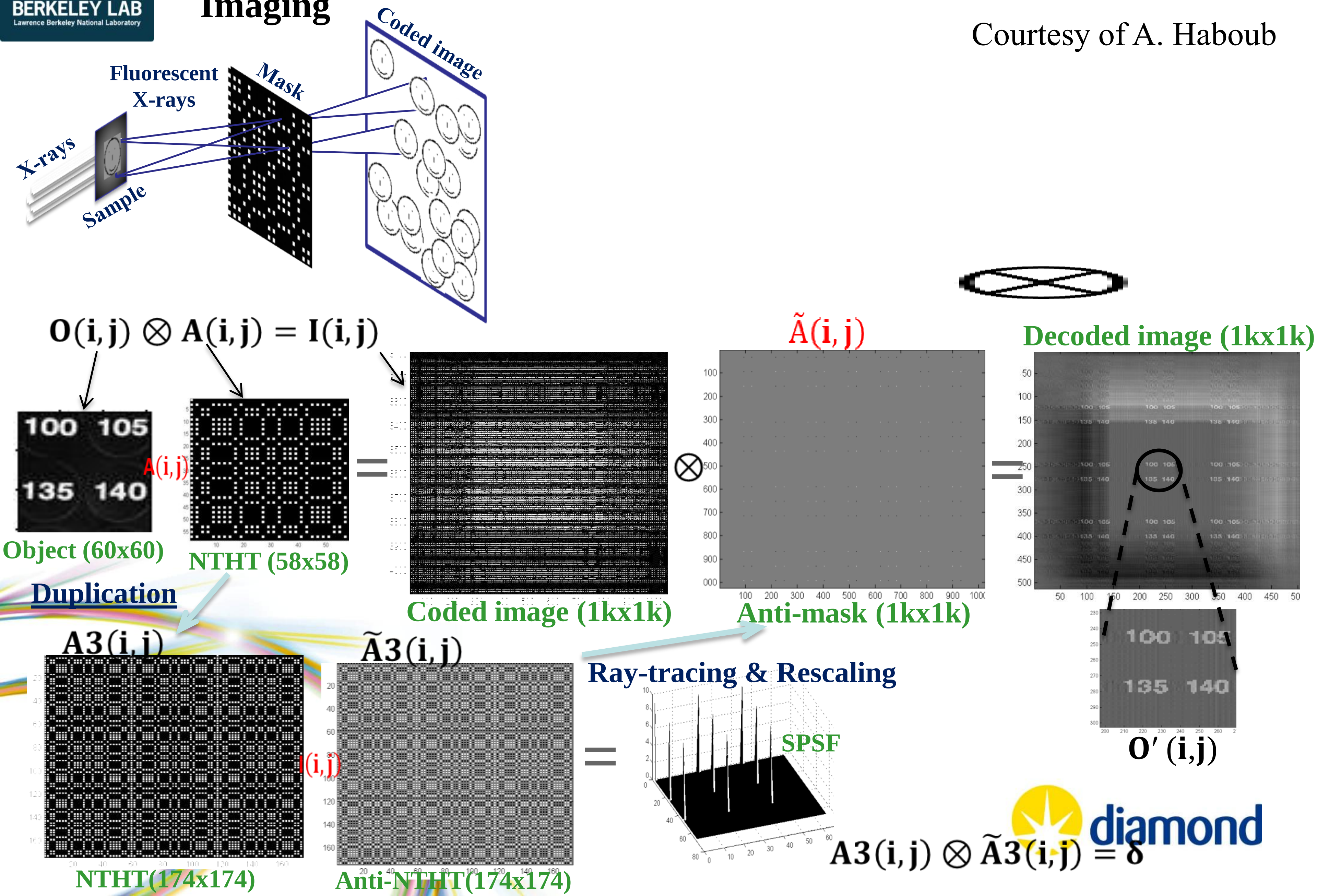

Coded Aperture Measurement Principles

R.H. Dicke, Astrophys. Journ., 153, L101, (1968).

- Coded Aperture Imaging:
  - Technique developed by x-ray astronomers using a mask to modulate incoming light. Resulting image must be deconvolved through mask response (including diffraction and spectral width) to reconstruct object.
  - Open aperture of 50% gives high flux throughput for bunch-by-bunch measurements. Heat-sensitive and flux-limiting monochromator not needed.
    - We need such a wide aperture, wide spectrum technique for shot-by-shot (single bunch, single turn) measurements.

E.E. Fenimore and T.M. Cannon, Appl. Optics, V17, No. 3, p. 337 (1978).

- URA (Uniformly Redundant Array) mask
  - Pseudo-random pattern gives relatively flat spatial frequency response.
  - In noiseless, geometric limit, detector image can in principle be inverted directly to give source profile
  - Unfortunately, we don't operate in that limit.
  - Need something like recursive or template fitting.
    - In this talk will discuss latter approach.

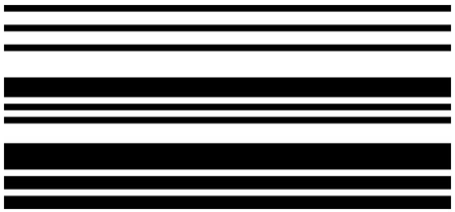

What the detector sees

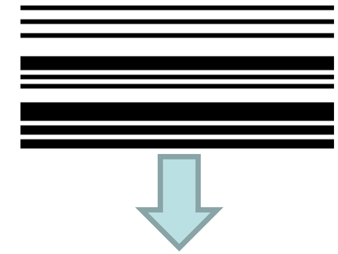

- Source SR wavefront amplitudes:

$$\begin{bmatrix} A_\sigma \\ A_\pi \end{bmatrix} = \frac{\sqrt{3}}{2\pi}\gamma\frac{\omega}{\omega_c}\left(1+X^2\right)(-i)\begin{bmatrix} K_{2/3}(\eta) \\ \frac{iX}{\sqrt{1+X^2}}K_{1/3}(\eta) \end{bmatrix},$$

where

$$X = \gamma\psi,$$

$$\eta = \frac{1}{2}\frac{\omega}{\omega_c}\left(1+X^2\right)^{3/2},$$

K.J. Kim, AIP Conf. Proc. 184 (1989).
J.D. Jackson, "Classical Electrodynamics," (Second Edition),John Wiley & Sons, New York (1975).

- Kirchhoff integral over mask
  (+ detector response)
  → Detected pattern:

$$A_{\sigma,\pi}(Detector) = \frac{iA_{\sigma,\pi}(Source)}{\lambda}\times \int_{mask}\frac{t(y_m)}{r_1 r_2}e^{i\frac{2\pi}{\lambda}(r_1+r_2)}\left(\frac{\cos\theta_1+\cos\theta_2}{2}\right)dy_m$$

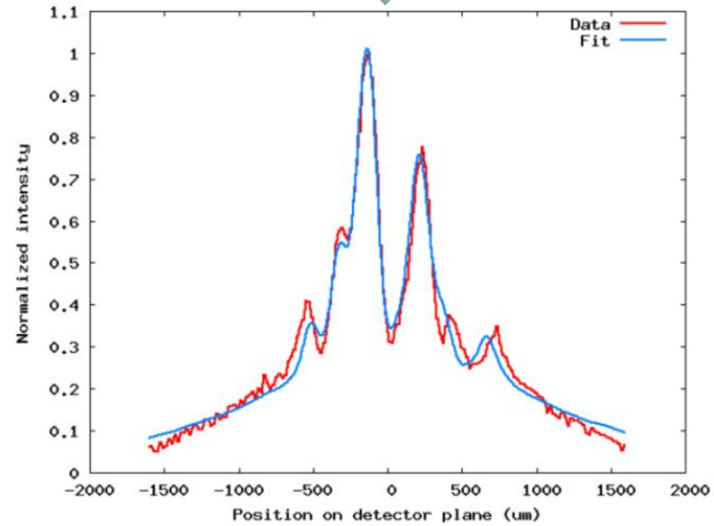

Measured slow-scan detector image (red) at CesrTA, used to validate simulation (blue)

- $t(y_m)$ is complex transmission of mask element at y_m.
- Sum intensities of each polarization and wavelength component.
- Sum weighted set of detector images from point sources.
  - The source beam is considered to be a vertical distribution of point sources.
  - Can also be applied to sources with non-zero angular dispersion and longitudinal extent, for more accurate simulation of emittance and source-depth effects.
  - For machines under consideration here these effects are small, so for computational speed we restrict ourselves to 1-D vertical distributions.

Measurements at CesrTA

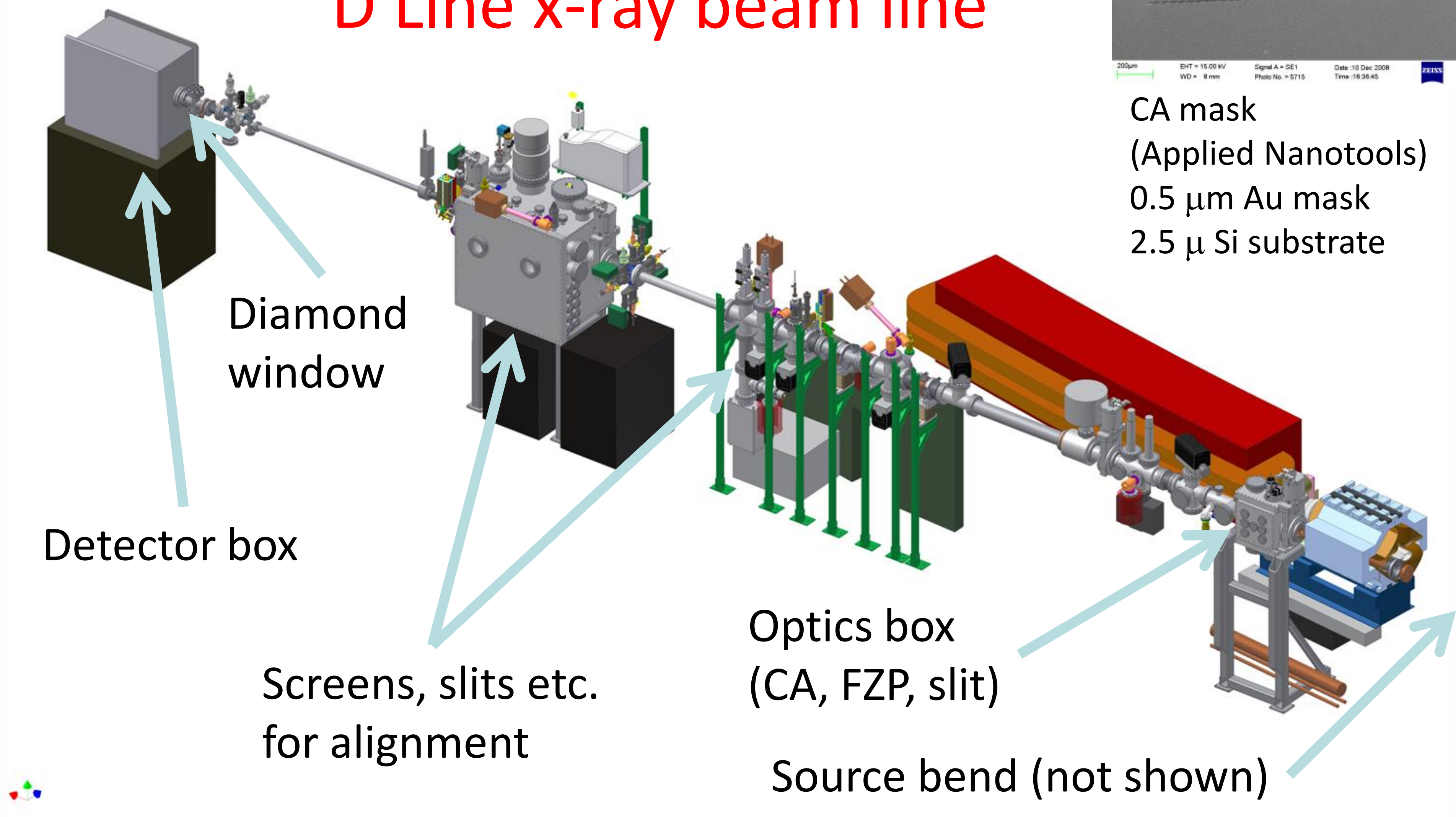

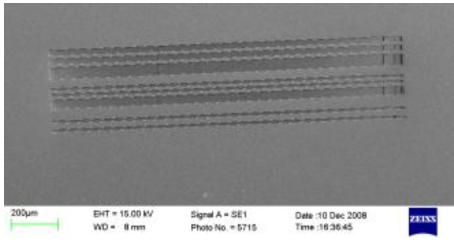

CA mask
(Applied Nanotools)
0.5 μm Au mask
2.5 μ Si substrate

10 μm, 31-element CA mask @ D Line 2 GeV

Generate detector images for various beam sizes:

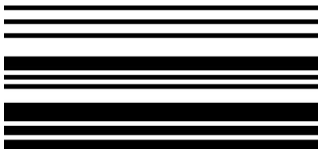

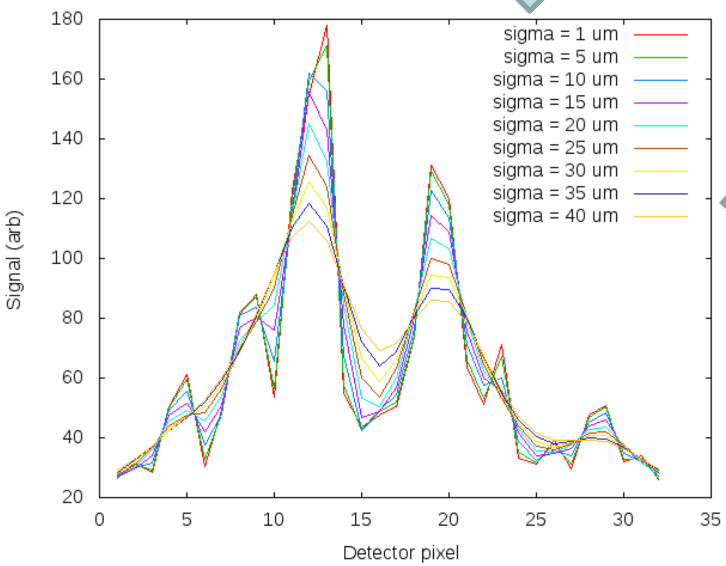

Cross-fit between beam sizes.
Plot 1-sigma statistical confidence regions,
Assuming 200 photons/pixel average
(=> 0.56 mA at 2 GeV):

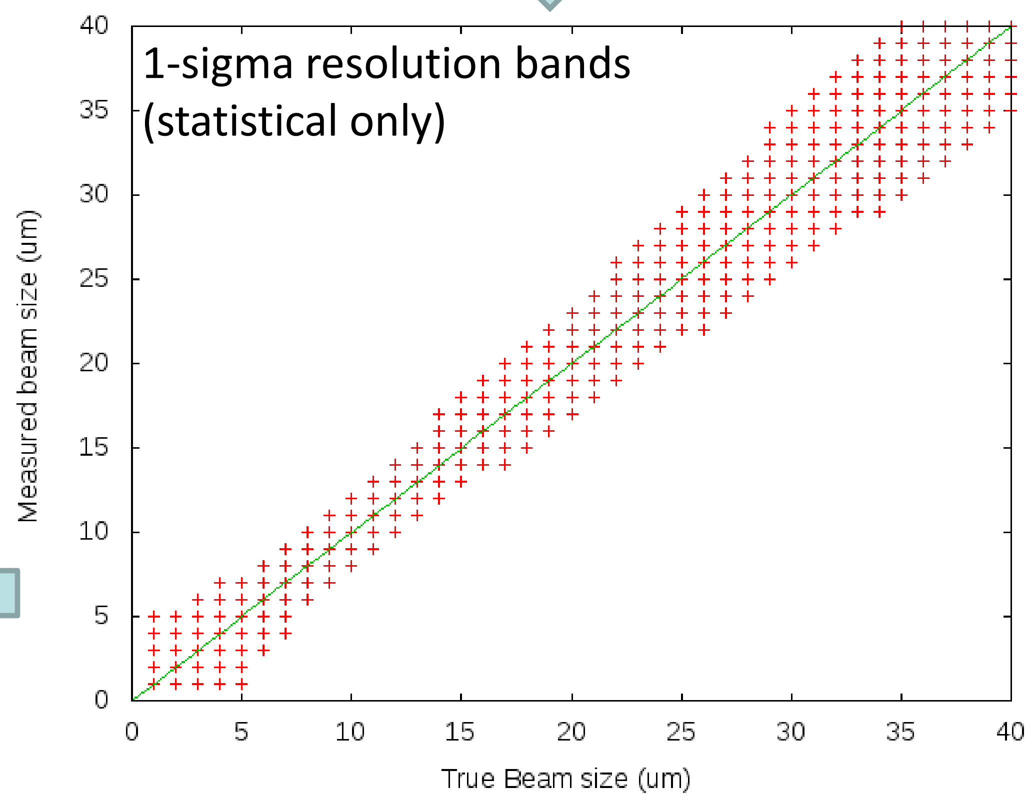

Statistical single-shot resolution at 10 μm beam size = +/- ~2 μm
(Assuming ideal detector.)

Data Analysis

- 1) Simulate point response functions (PRFs) from various source positions to detector, taking into account beam spectrum, attenuations and phase shifts of mask and beamline materials, and detector response.
- 2) Add PRFs, weighted to possible proposed beam distributions.
- 3) Find best fit to detector data.

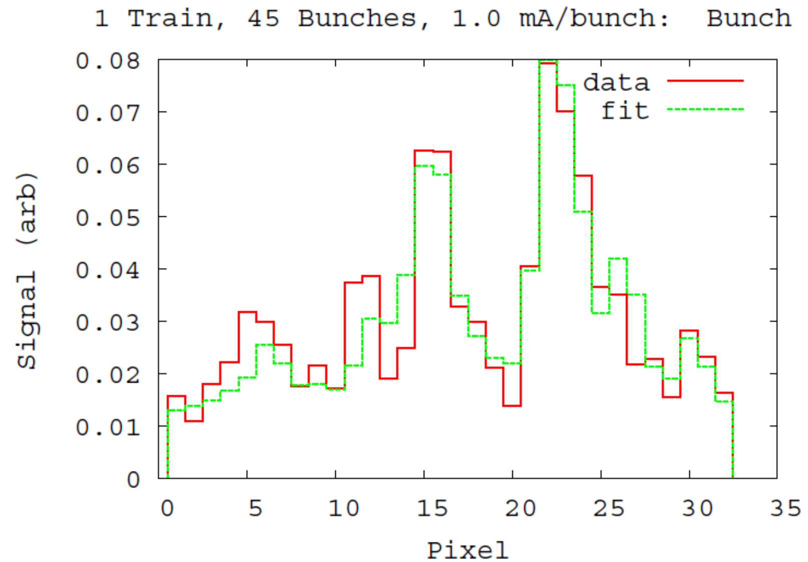

Example of single-shot data (single-bunch, single-turn)

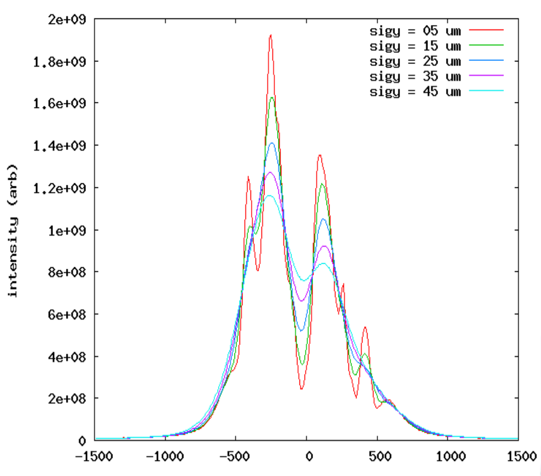

Simulated detector image for various beam sizes at CesrTA

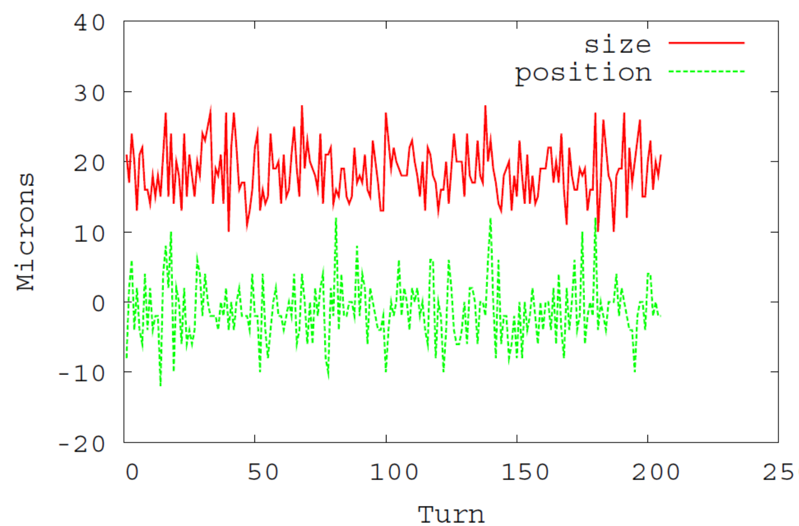

Example of turn-by-turn data (one bunch out of train)

Electron-cloud study data

- Study of how of electron clouds change bunch-by-bunch beam sizes along a train.
- Beam sizes down to ~10 μm have been measured at CesrTA.

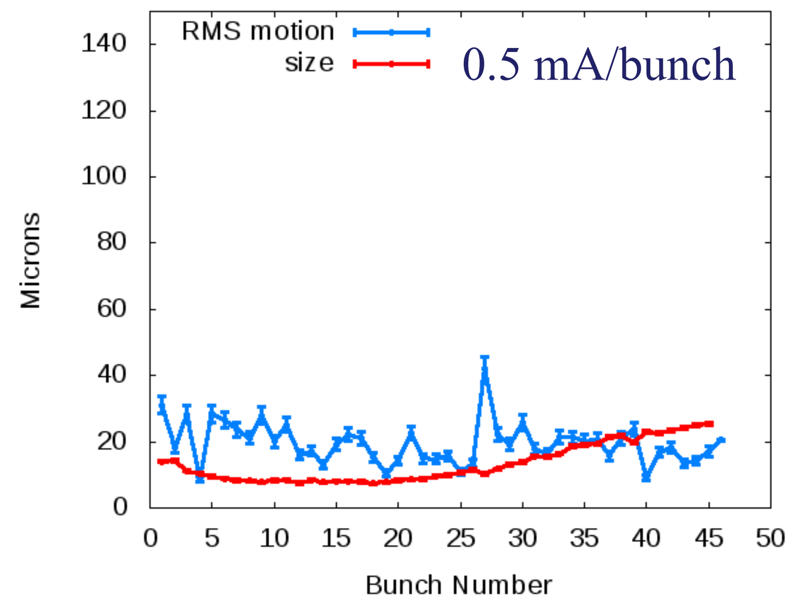

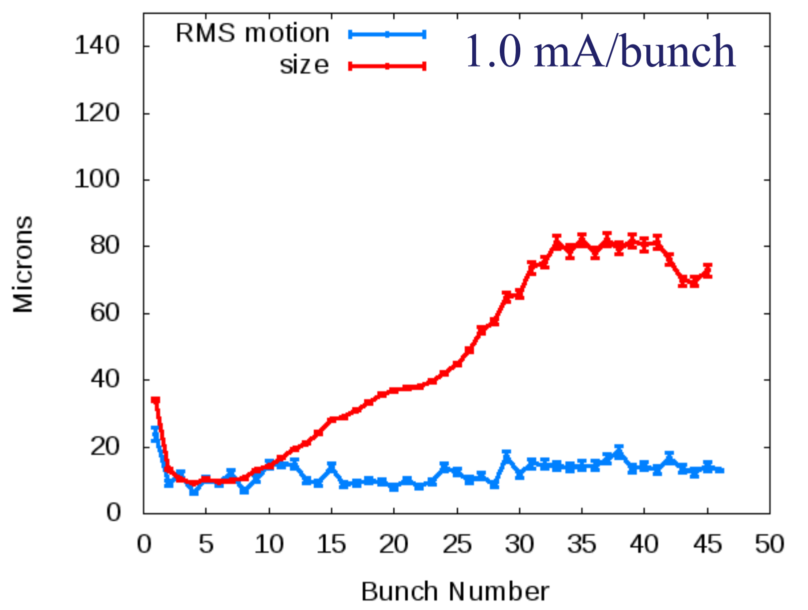

Coded Aperture tests at ATF2

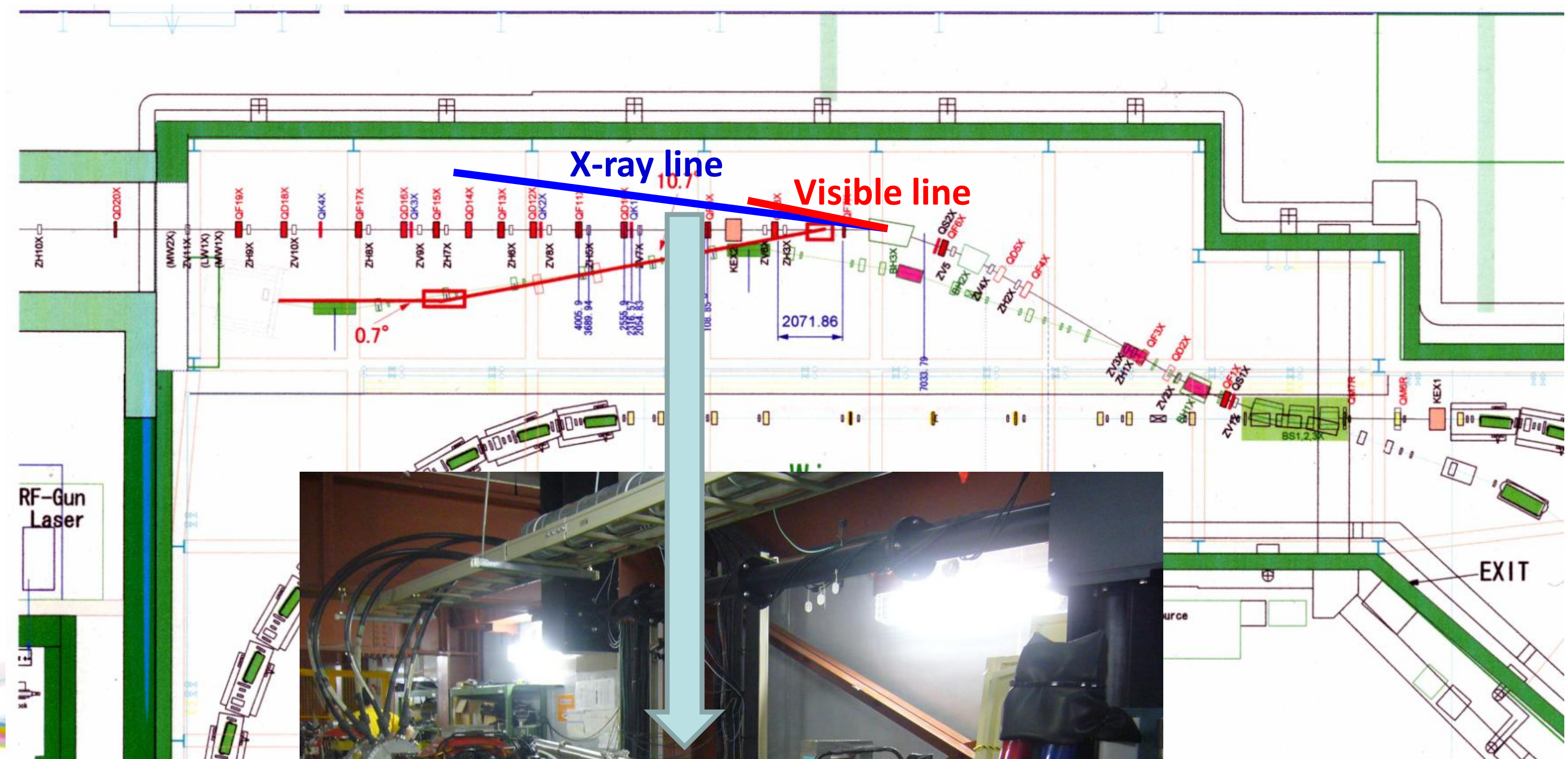

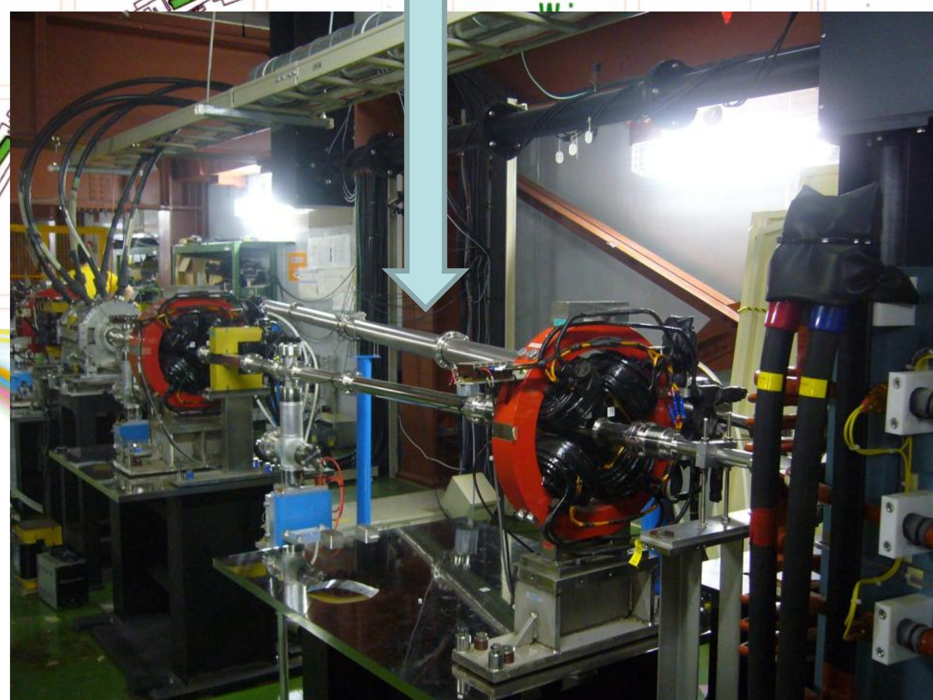

47-element, 5 μm/element URA mask @ ATF2

Generate detector images for various beam sizes:

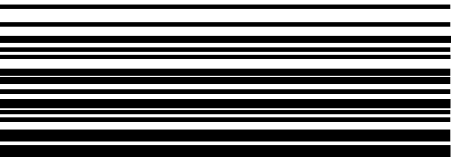

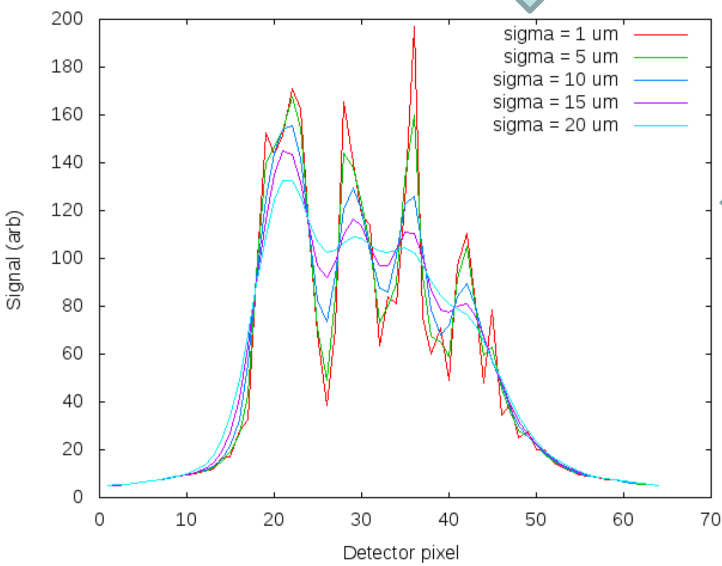

Cross-fit between beam sizes.
Plot 1-sigma statistical confidence regions,
Assuming 200 photons/pixel (average):

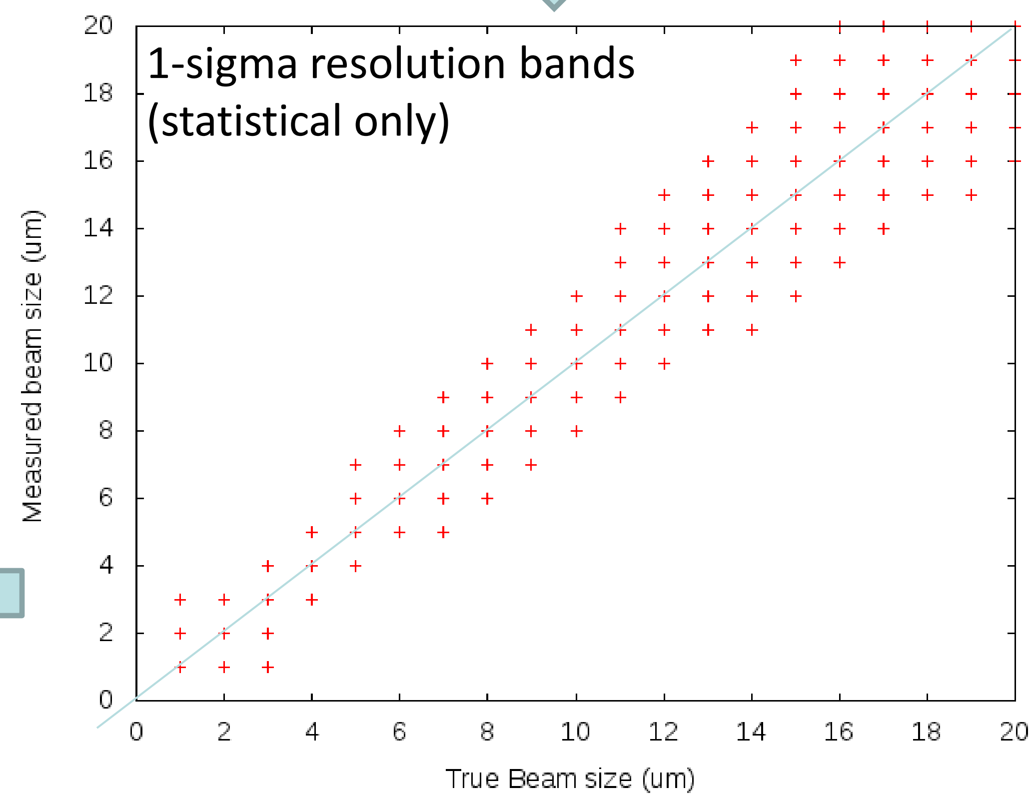

Statistical single-shot resolution at 4 μm beam size = +/- ~1 μm
(Assuming ideal detector.)

- Fresnel Zone Plate:
  - Construction:
    - Alternating zones from opaque to transparent with their radii r_n as:

      $r_n^2 = n \lambda f + n^2 \lambda^2 / 4$
  - Resolution:
    - $R = 1.22\, \Delta r_N$
  - Fraction of power focussed (classical expression based on 100% absorption and 100% transmission):
    - $E = 1/(q\pi)^2$, q =1,2,3,etc. and E = 0.25 for q=0
      - First order max diffraction efficiency: 10.3%

- Performance of FZP
  - Improved performance by the choice of material and also manufacture process
  - Resolution: Δr outer rings radii difference
  - Depth of field: l / NA^2
  - Efficiency: material and thickness
  - Aberrations: imperfection of the lens, NA
- Construction tolerance:
  - resolution and efficiency: high aspect ratio

- FZP diffraction efficiency for Au, taking into account phase effects of the absorbing material

$$E = \left(\frac{1}{\pi q}\right)^2 \left(1 + e^{-4\pi\frac{T\beta}{\lambda}} - 2e^{-2\pi\frac{T\beta}{\lambda}} \cos 2\pi\frac{T\delta}{\lambda}\right)$$

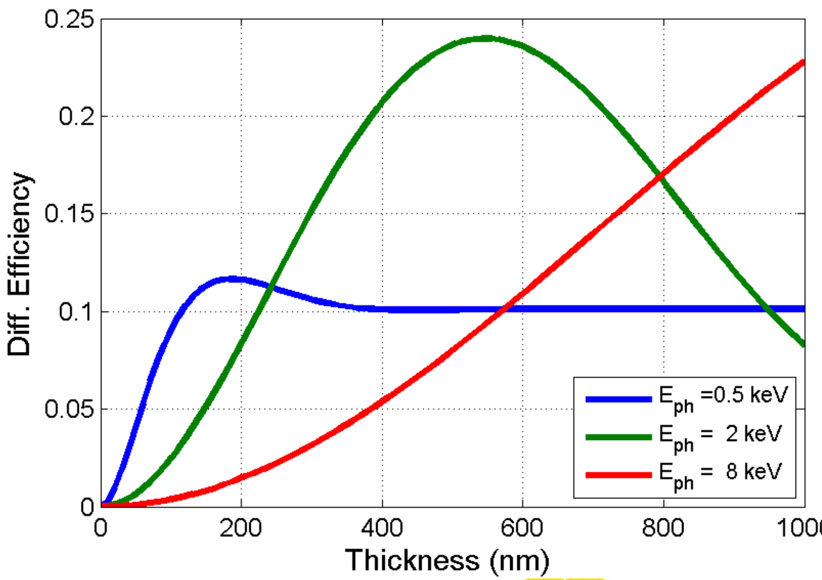

Syue-Ren Wu *et al*
Materials 2012, 5, 1752-1773; doi:10.3390/ma5101752

- Examples of FZP with X-ray beam
  - Beam size measurement: KEK, Spring8, etc
    - Achieved measured beam size, ATF-KEK: 4μm
  - Beam focussed for X-ray experiment
    - Achieved image beam size: 20nm

Courtesy of Dr. J. Vila-Comamala

Fresnel Zone Plates

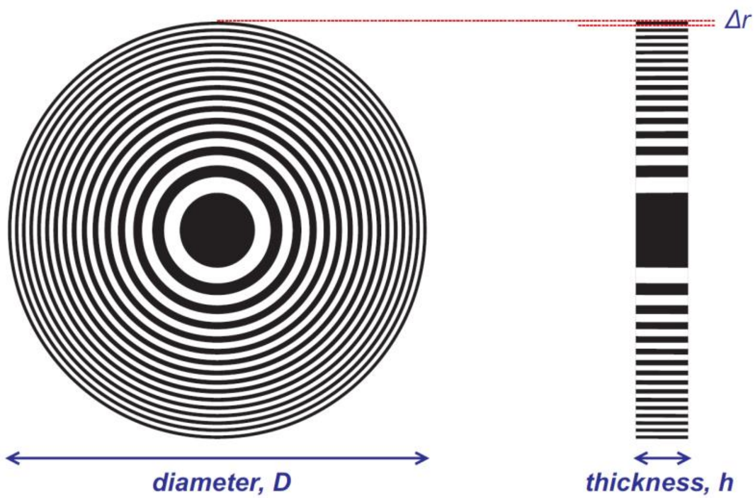

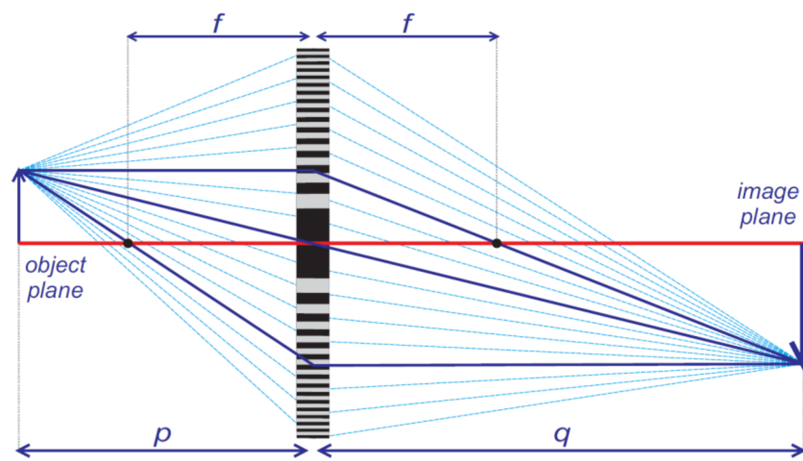

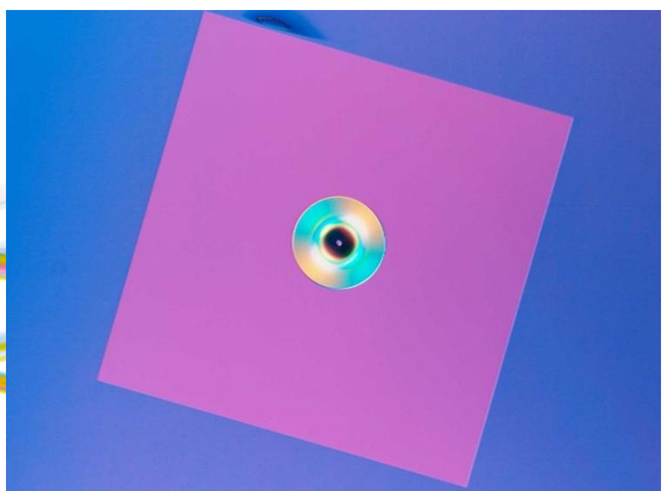

Fresnel zone plate on Si_3N_4 membrane

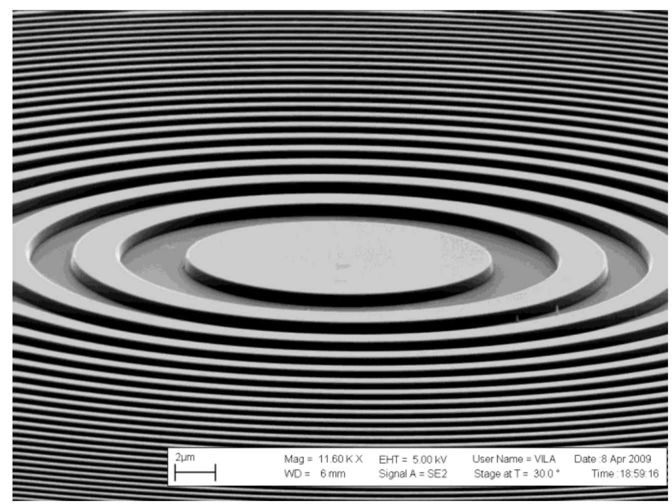

SEM image of Fresnel zone plate

Courtesy of Dr. J. Vila-Comamala

Fresnel Zone Plate Modeling: Zone-doubling

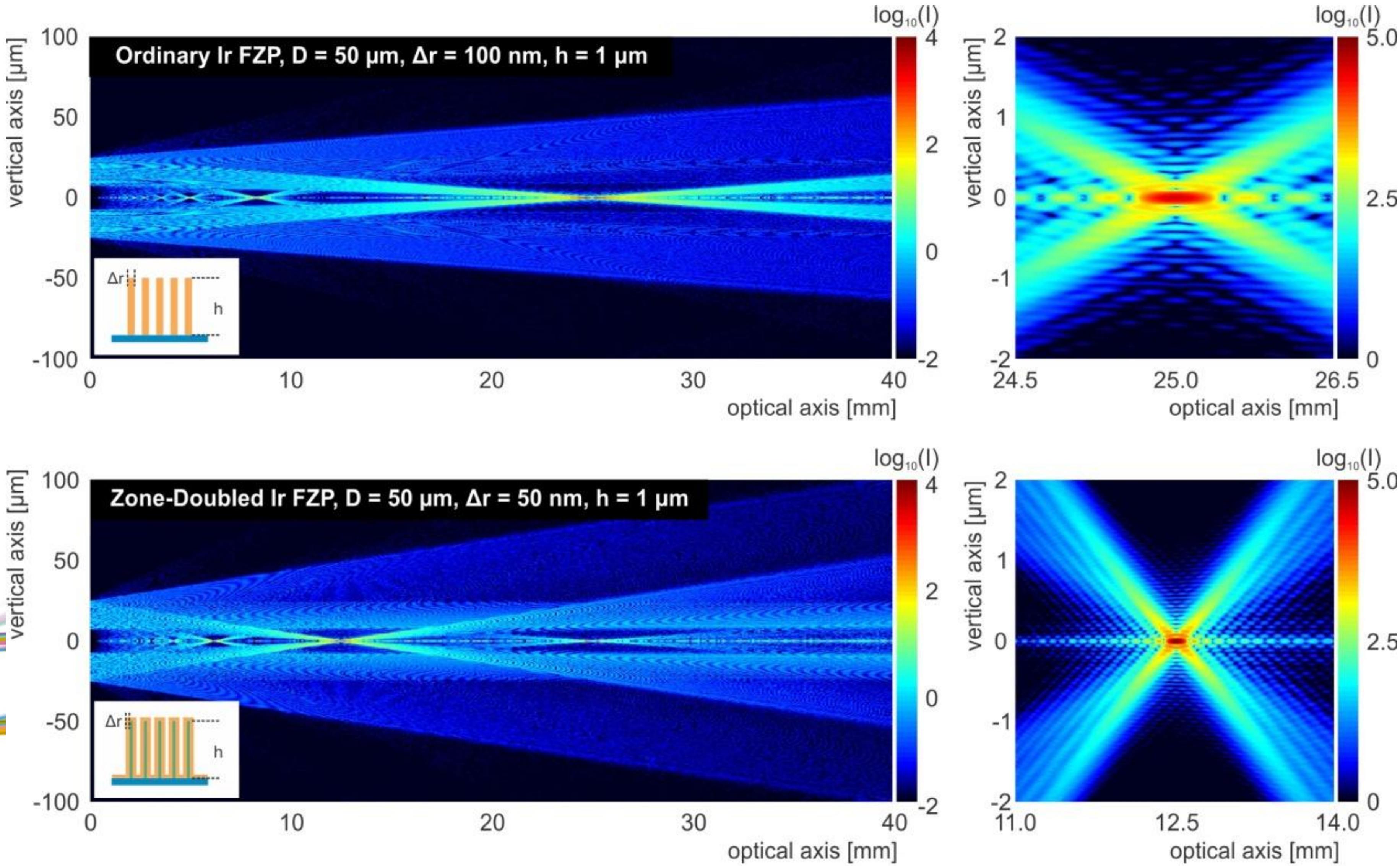

J. Vila-Comamala et al., J. Synchrotron Rad. (2010)

diamond

Courtesy of Dr. J. Vila-Comamala

Fresnel Zone Plate Modeling: Zone-doubling

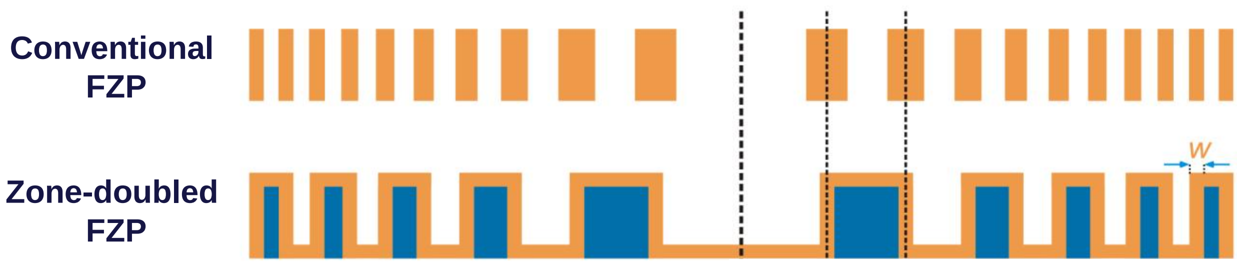

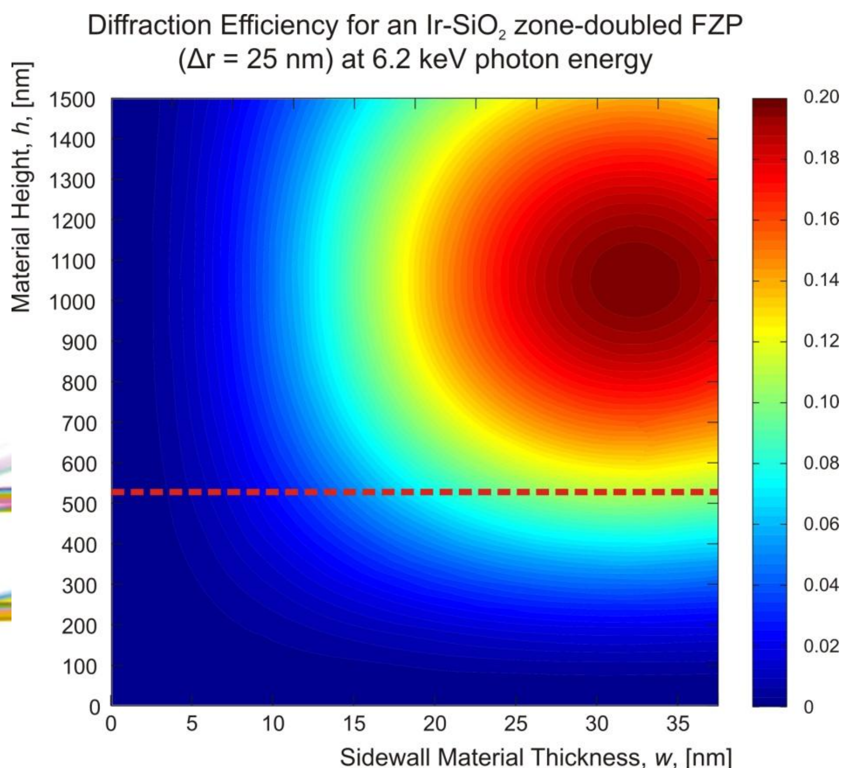

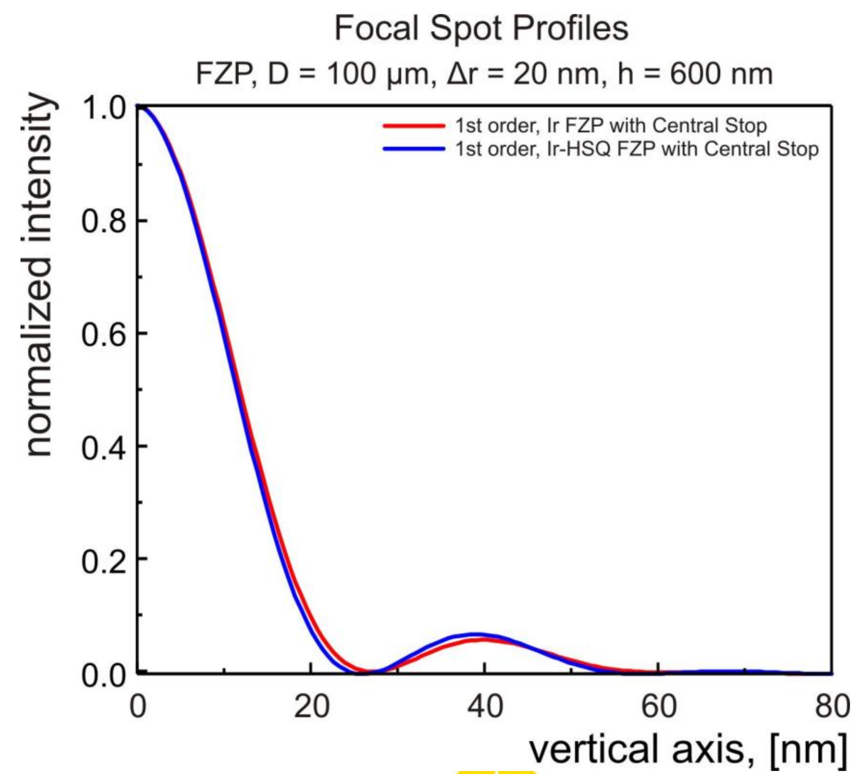

Courtesy of Dr. J. Vila-Comamala

Nanofabrication techniques transferred to ANL-CNM from the Paul Scherrer Institut (Switzerland)

Au electroplating

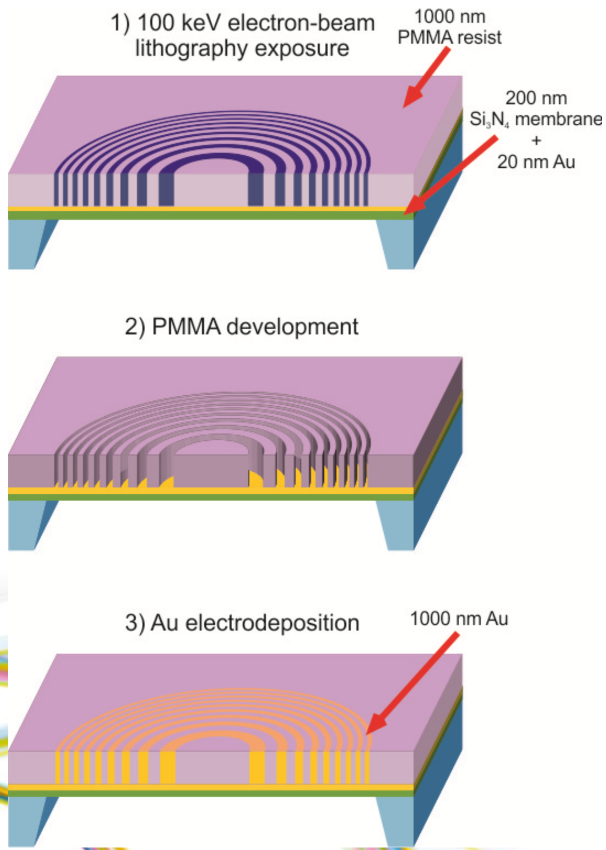

S. Gorelick et al., Nanotechnology (2010)

Zone-doubling technique

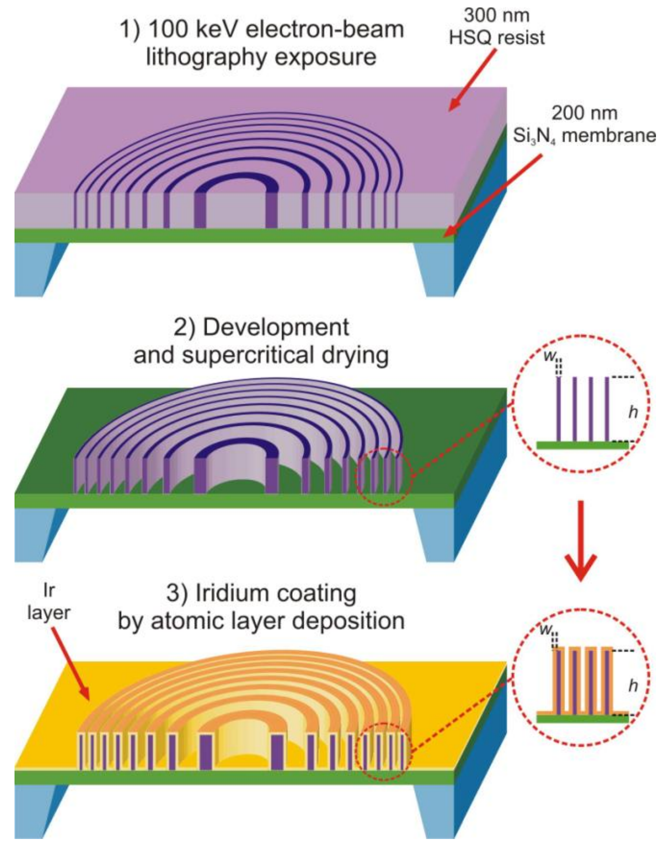

J. Vila-Comamala et al., Nanotechnology (2010)

J. Vila-Comamala et al., Optics Express (2011)

Au FZP for 8-12 keV photon energy

FZPs for sub 100-nm focusing

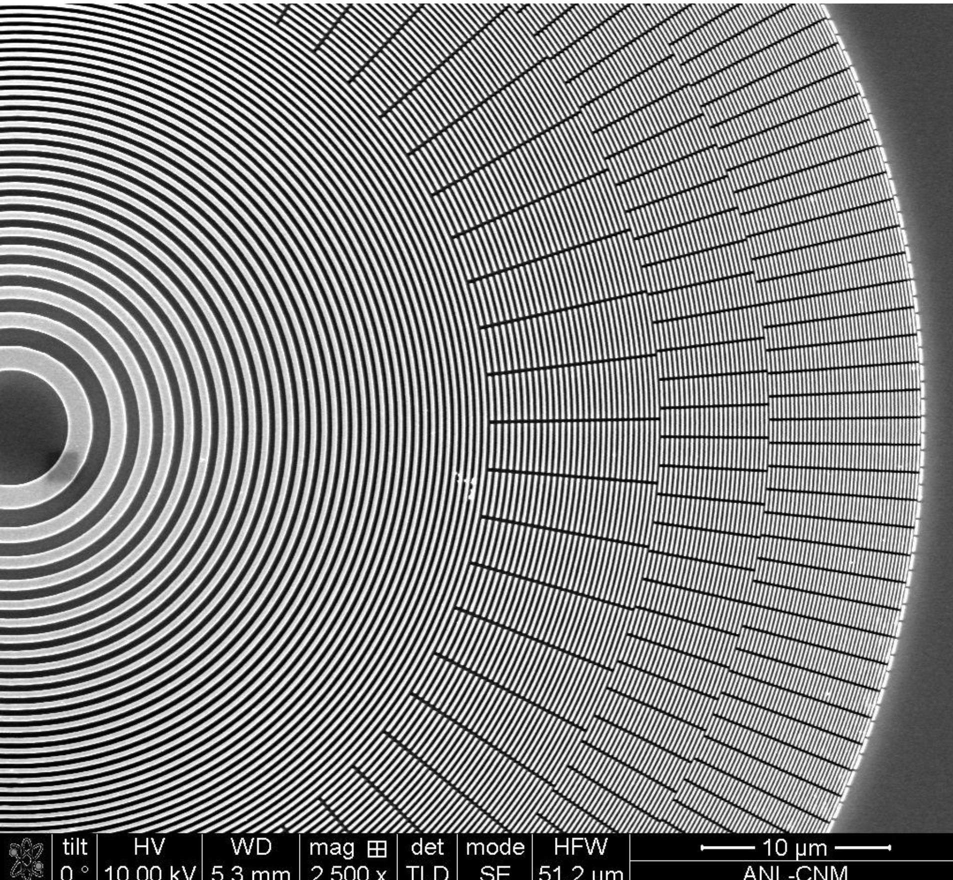

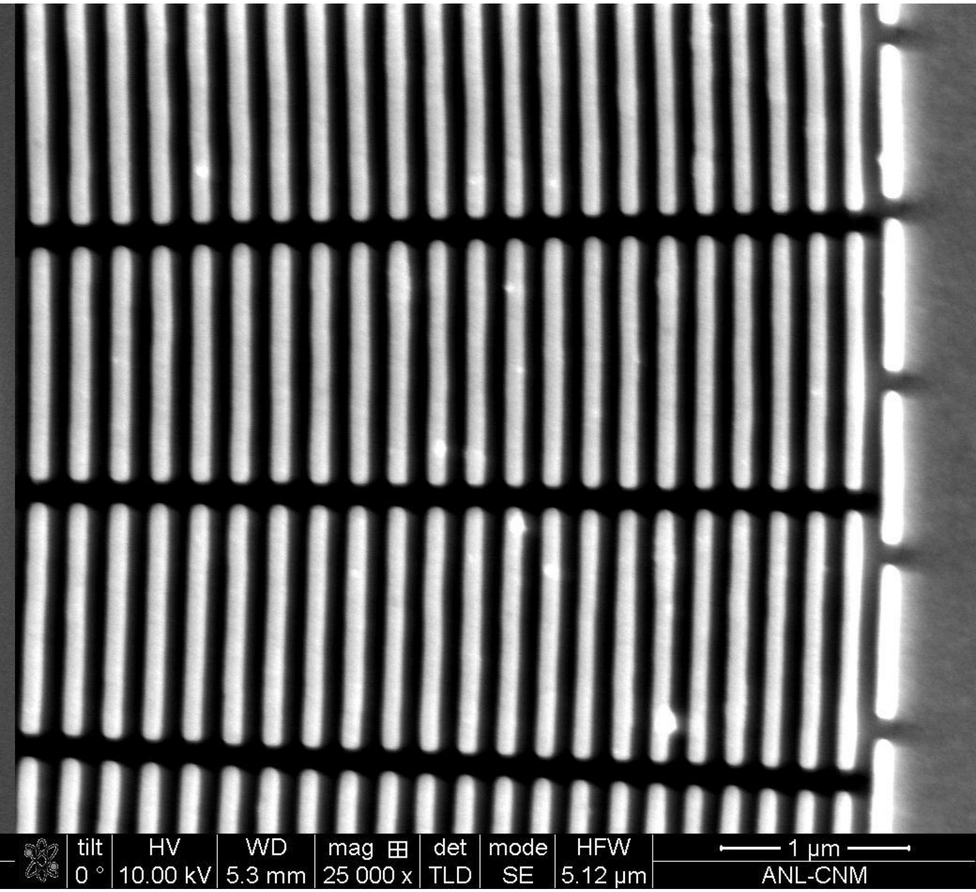

Au FZP, D = 100 um, dr = 100 nm, t ~ 900 nm

diamond

20 nm Ir lines / 40 nm period d
after Ir ALD

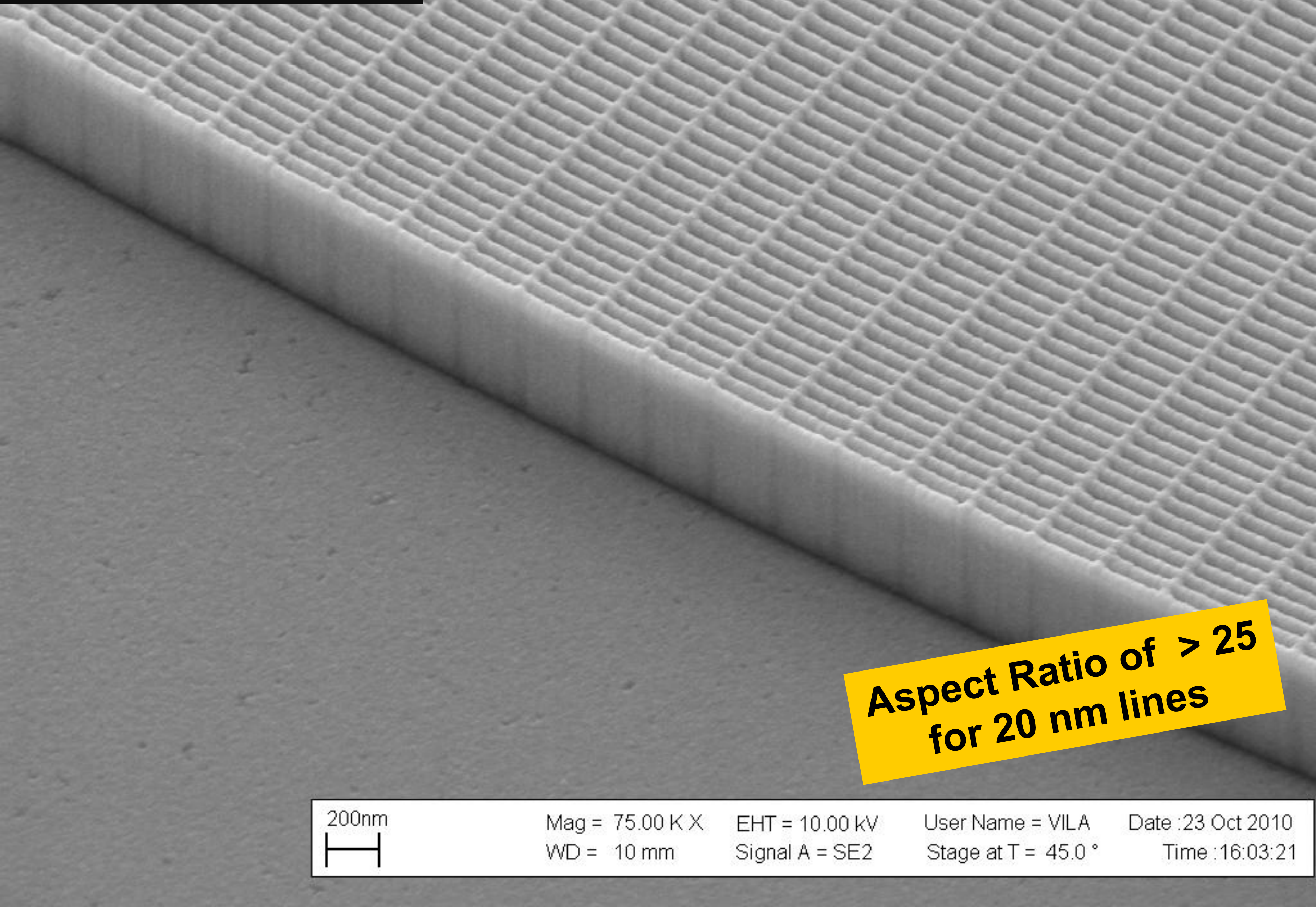

Courtesy of Dr. H. Sakai

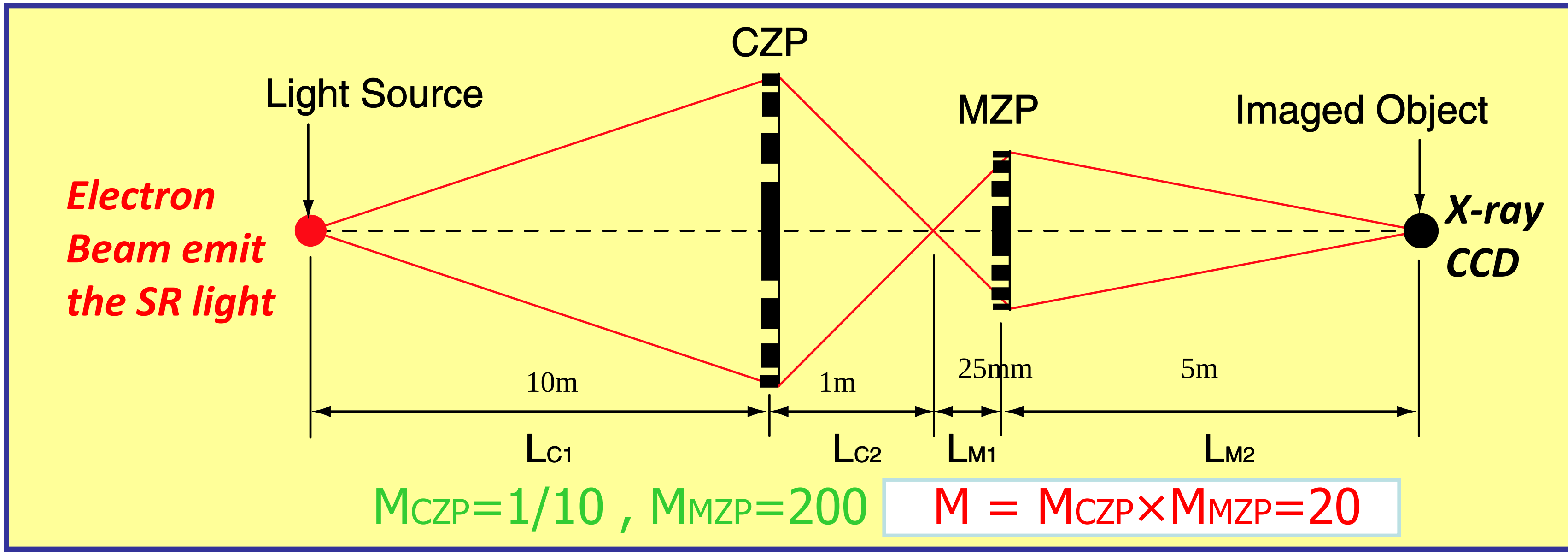

Features

1) High spatial resolution (<1 μm)
2) Non-destructive measurement
3) 2-dimentional (x,y) beam profiling
4) Real time beam profile mesurement (<1ms)

Expected spatial resolution

Parameters	Definition	Resolution(1σ)
Diffraction limit (3.235keV)	$\lambda/4\pi\sigma SR$	0.24 [μm]
CZP (Δr_N=116nm)	σCZP / MCZP	0.55 [μm]
MZP (Δr_N=124nm)	σMZP / (MCZP × MMZP)	0.002 [μm]
CCD (1 pixel=24μm×24μm)	σCCD / (MCZP × MMZP)	0.35 [μm]
Total	--	0.7 [μm]

Courtesy of Dr. H. Sakai

FZP monitor was installed at KEK-ATF damping ring.
Expected beam sizes are
Horizontal : 50μm、 Vertical : <10μm

Setup

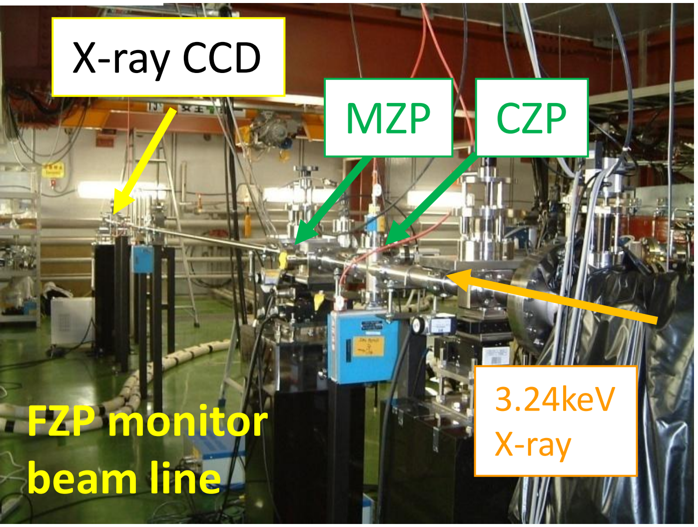

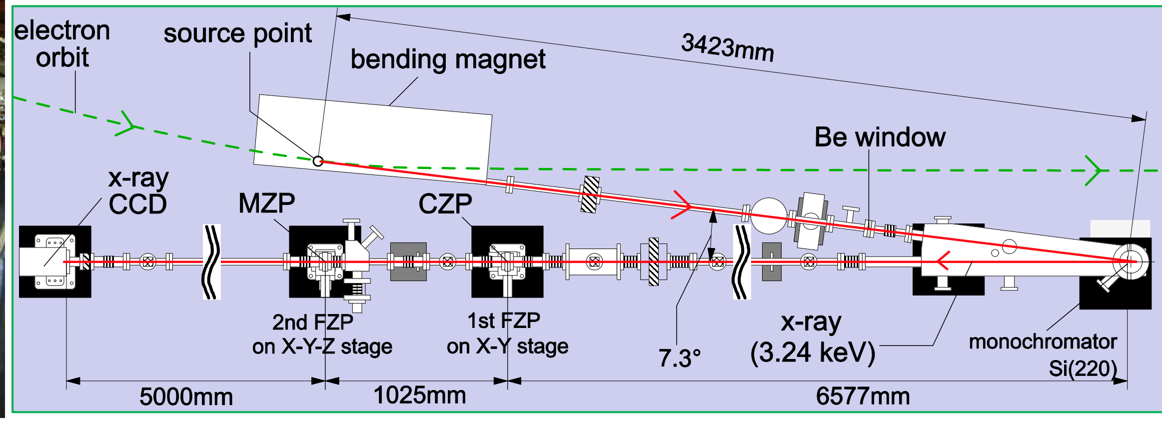

Results

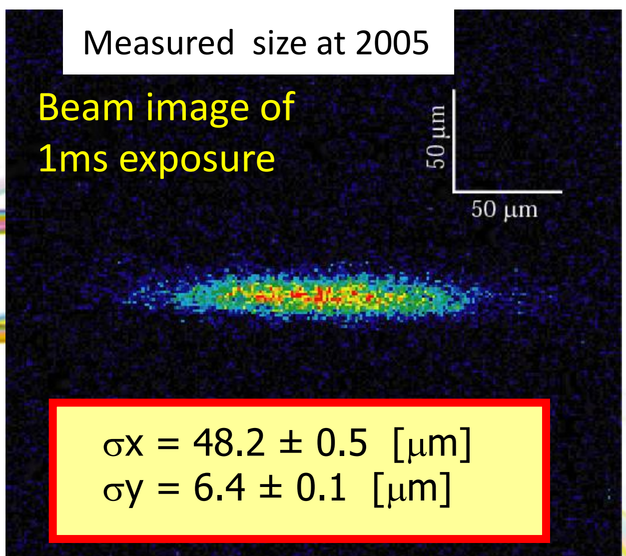

H.Sakai et al. PRST-AB 10,041801 (2007)

Recently , by removing the vibration source come from air compressor near Si monochromator, 100Hz vibration disappeared and less than 4um vertical beam size was measured.

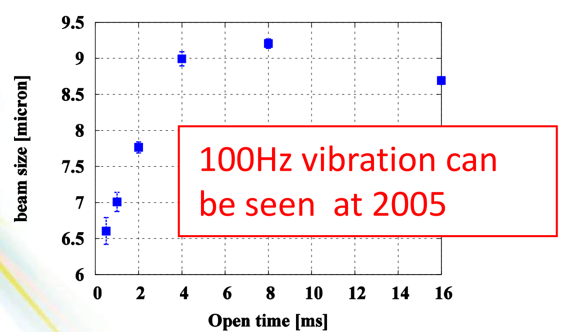

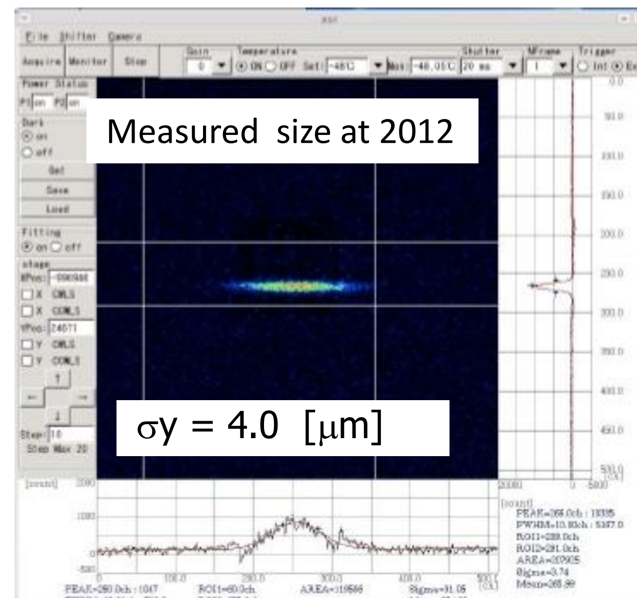

T.Naito et al. Proc. of IBIC2012, (MOPB63

CRL Lenses

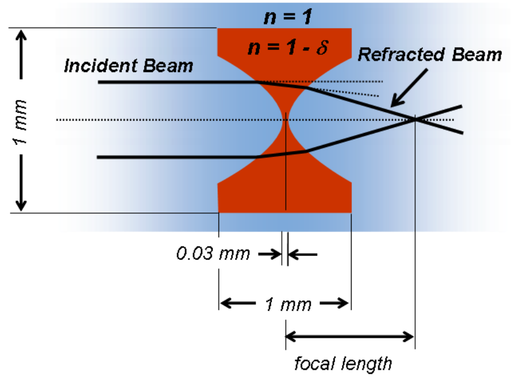

- Principle:
  - Focal lens depends on material and wavelength λ:

$$F = \frac{R}{2N\delta} \qquad \delta = \frac{r_0}{2\pi}\lambda^2 N_{at}\frac{mZ}{a^3}$$

  - Absorption: depends on material

    - low Z material makes low absorption
    - high Z material makes short focal length

CRL Lenses

ESRF | *RWTH Aachen*

Microscope images

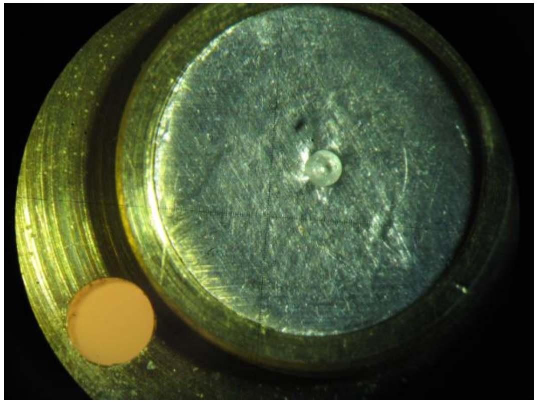

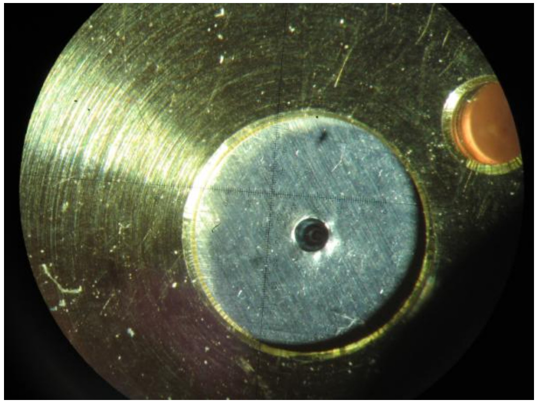

phase contrast imaging

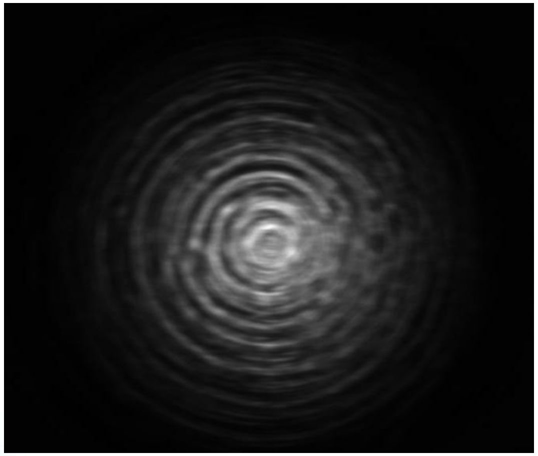

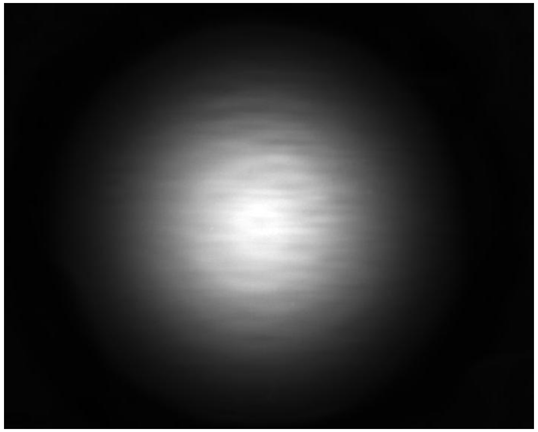

Measure and
computed lens aperture

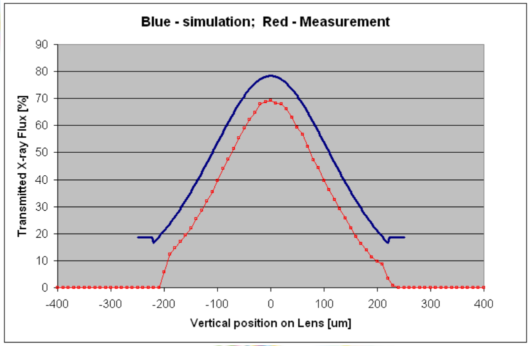

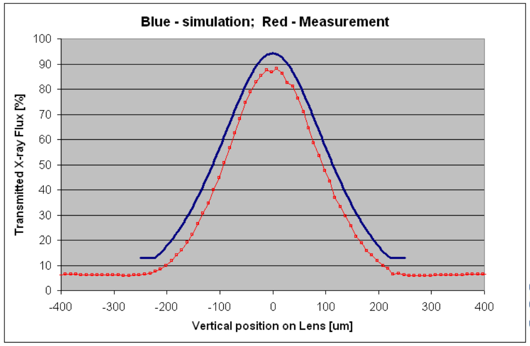

- Resolution:
  - PSF from ‘perfect aperture’ calculated from absorption measurement

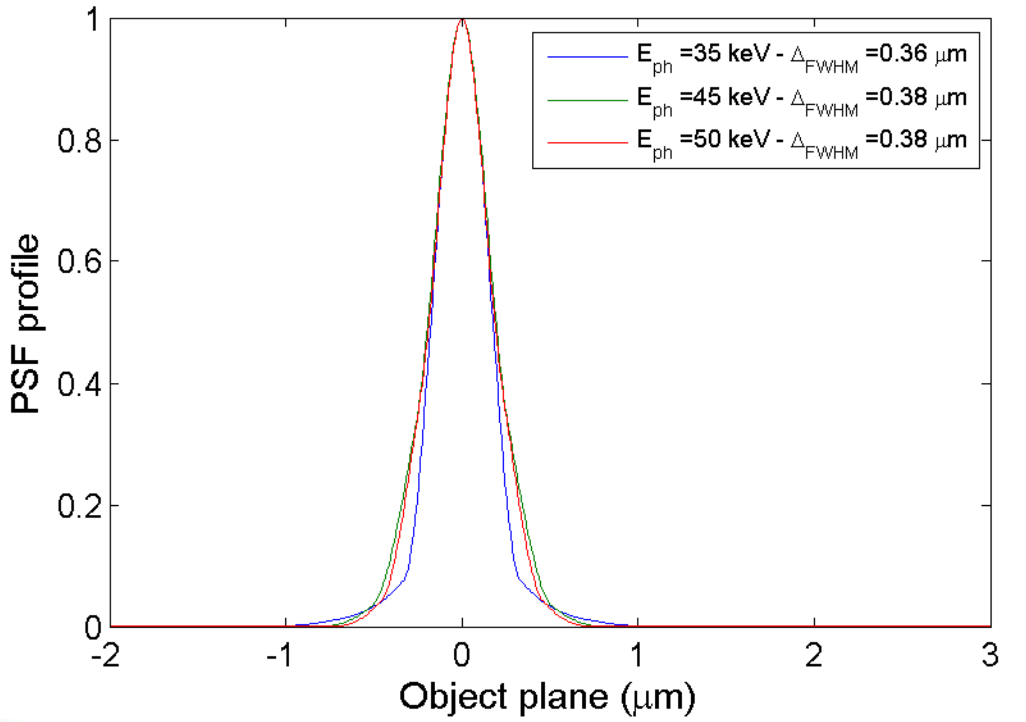

- ESRF beam
  - $\sigma_{x,y} = 84, 14\ \mu m$
  - emittance: $\varepsilon_x \approx 4.5$ nm.rad
  - $\varepsilon_y \approx 5$ pm.rad

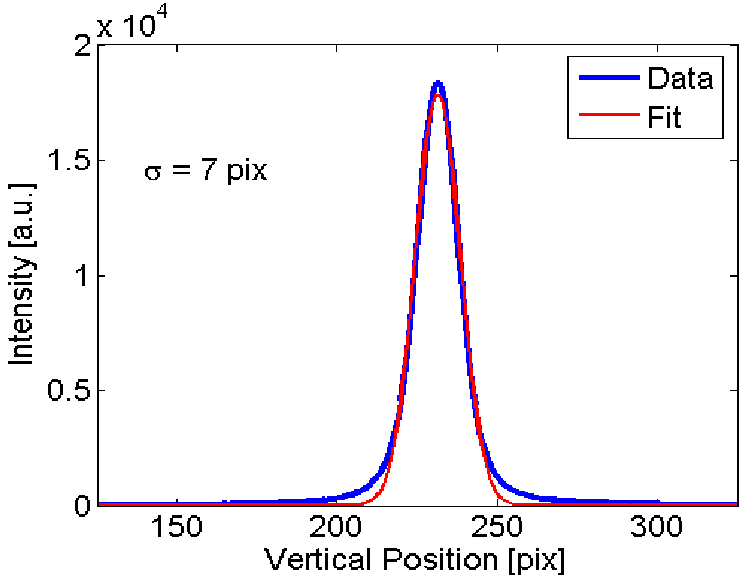

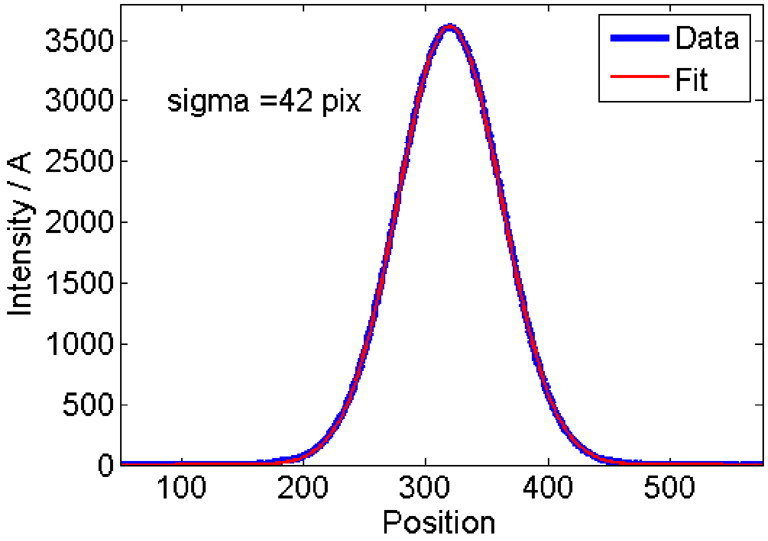

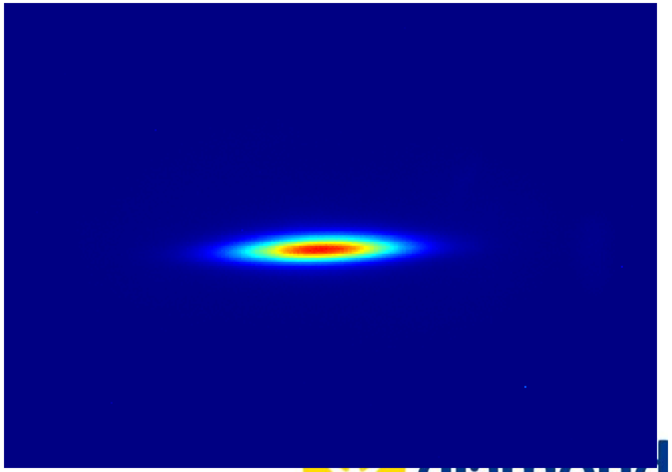

CRL Lenses

- Beamline I11 (Diamond)

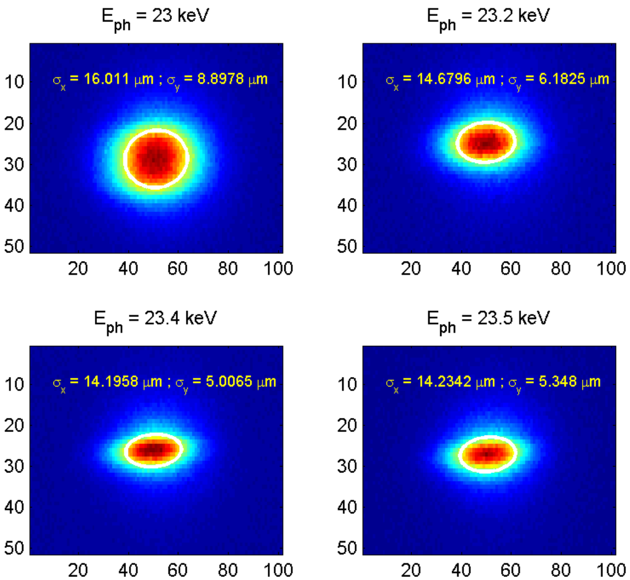

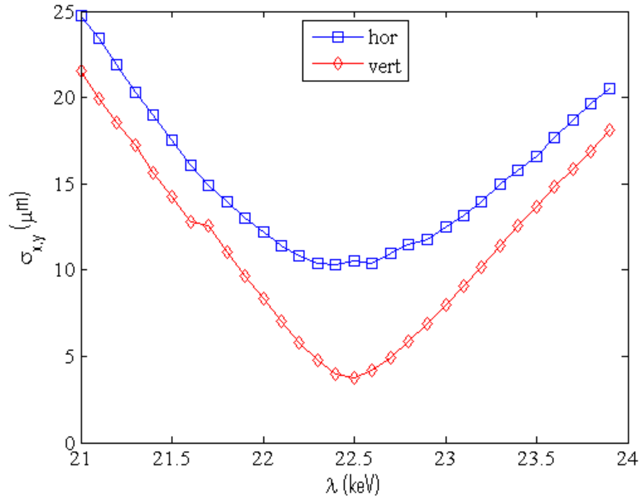

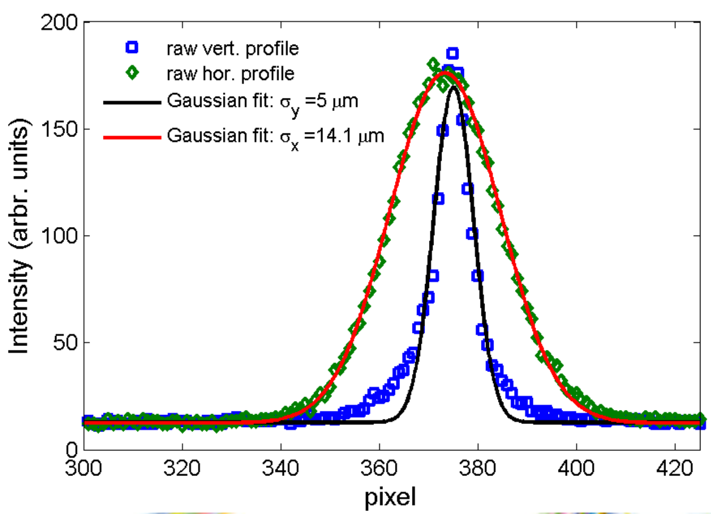

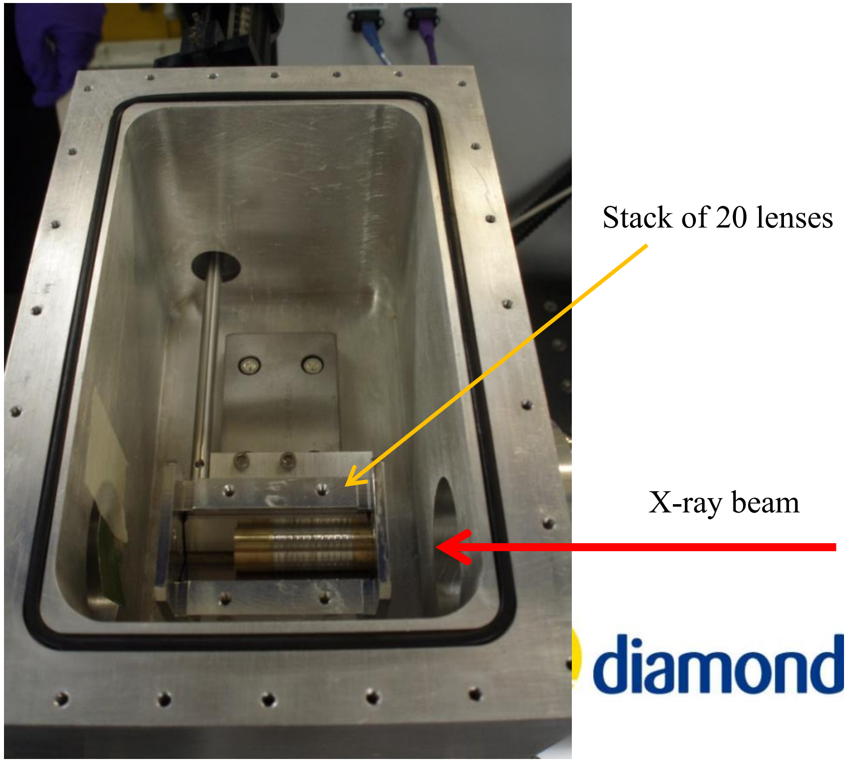

diamond

Other Beam Profile Diagnostics

- Visible light, quasi-homogeneous source:
  - interferometer: 4.7 μm vertical beam size (T. Mitsuhashi - ATF KEK)
  - π-polarisation: 3.5 μm vertical beam size (V. Schlott-PSI)
- X-ray pinhole camera:
  - 5 μm, (C Thomas – Diamond)

Commissioning, Operation, Cost, Performance

	Monochromatic	BM Resolution	Trans. Flux	Cost
CRL	Yes	Yes	Al ~80% of the illuminated aperture	+++
FZP	Yes	Yes	Max 25% of the illuminated aperture	+++
MURA	No	Yes/No	50% of the illuminated aperture	++
Pinhole camera	No	No	Fraction of the total flux	+
interferometer	Yes	Yes	Fraction of the total flux	+

Concluding remarks

- Sources reaching micron size in near future:
  - need to take into account the coherence of the source and more sophisticated model is needed to design profile monitors.
- Resolution of large aperture X-ray profile monitors can reach the natural resolution limit from the beam
  - Deconvolution can help to retrieve the real source profile: example of the X-ray pinhole showed that very small source size can be imaged with rather large aperture, assuming an accurate model of the PSF
- MURA etc., offer micron size resolution and high sensitivity, but processing of the image is required
- FZP and CRL have probably the best resolution, but they are not very sensitive - absorption or low efficiency, but also need monochromatic beam
  - Monochromatic beam imposes additional cost and effort for commissioning and operation
- Other possible profile measurement may be considered and compared to in terms of resolution, cost, commissioning, operation and maintenance

- Many thanks to
  - Diamond Diagnostics group (Chris Bloomer, Alun Morgan, Graham Cook) and Accelerator group (Dr. Riccardo Bartolini, Dr. Ian Martin)
  - Dr. Hiroshi Sakai (KEK)
  - Dr. Joan Vila-Comamala (Diamond)
  - Dr. Abdelmoula Haboub, Dr. Dula Parkinson (LBNL)
  - Dr. Gianluca Geloni (DESY)

Back up Slides

X-ray Pinhole PSF

- Pinhole PSF in the near field:
  - Fresnel diffraction integral
  - Weighted sum over the power spectrum in the screen
  - Convolve the PSF with the camera PSF

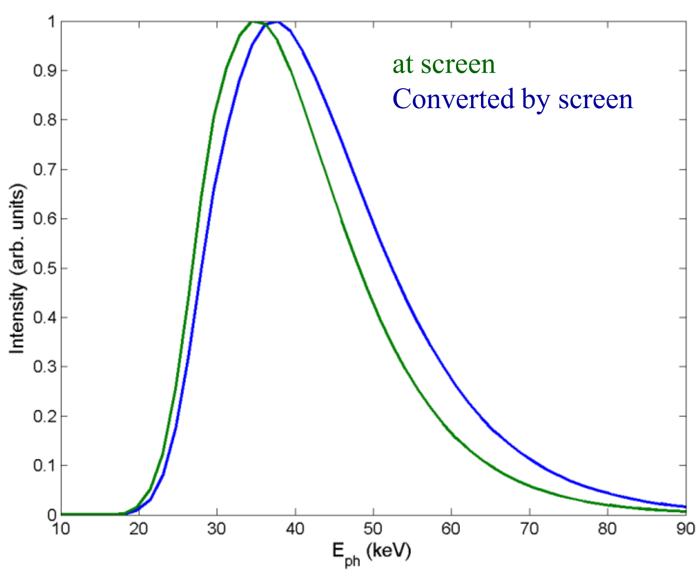

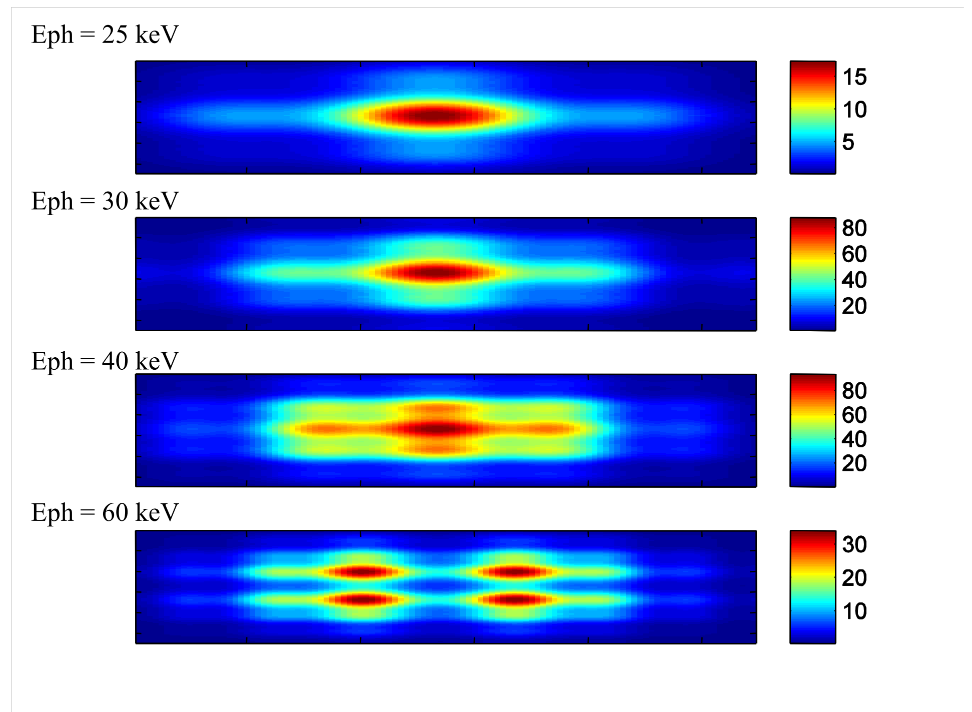

PSF of the X-ray pinholes

- Case of Diamond: Diagnostics Pinholes 1
- PSF for several square apertures

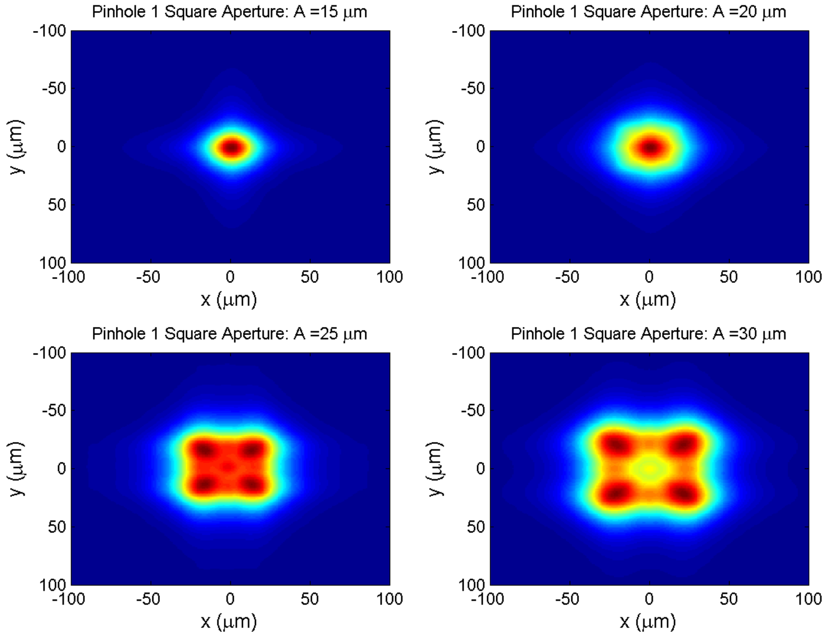

PSF of the X-ray pinholes

- Case of Diamond: Diagnostics Pinholes 1
- PSF for several circular apertures

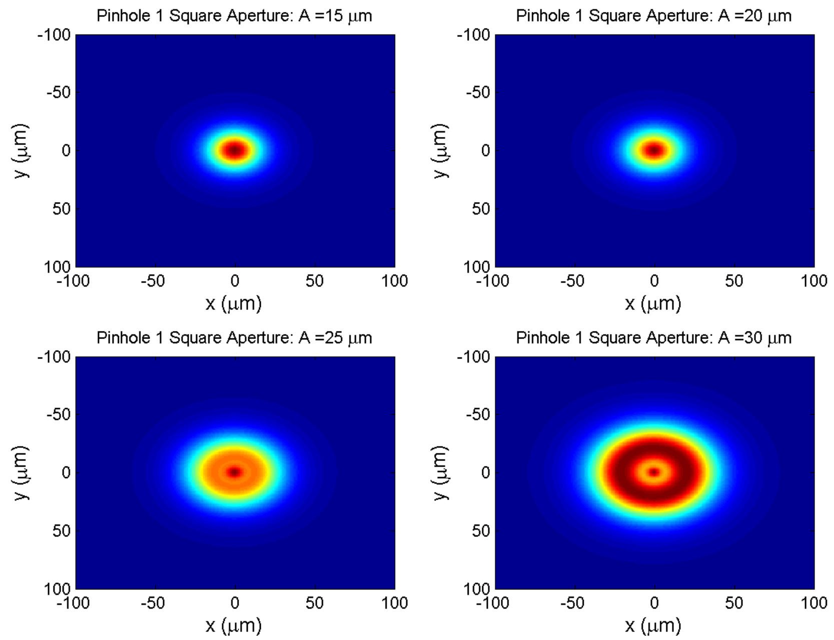

Deconvolved beam size with a range of defined apertures

- Beam size measured on raw images and on deconvolved images of both pinholes, for the same K

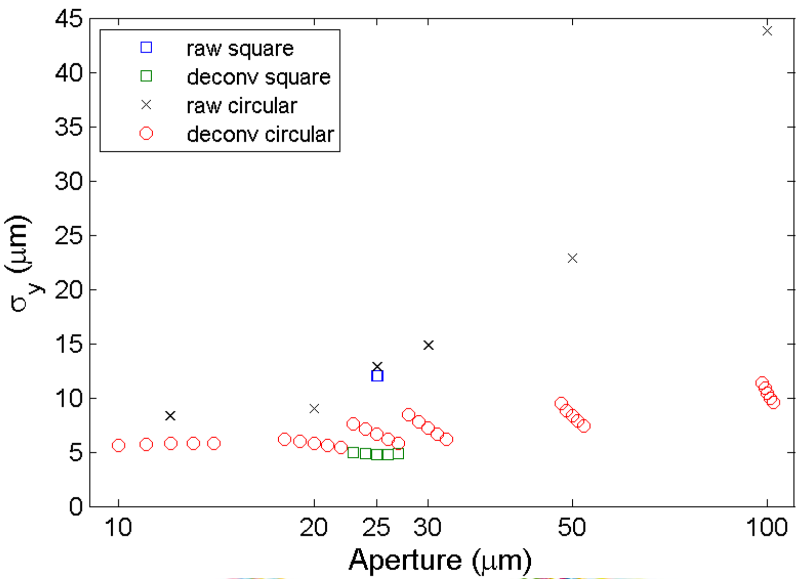

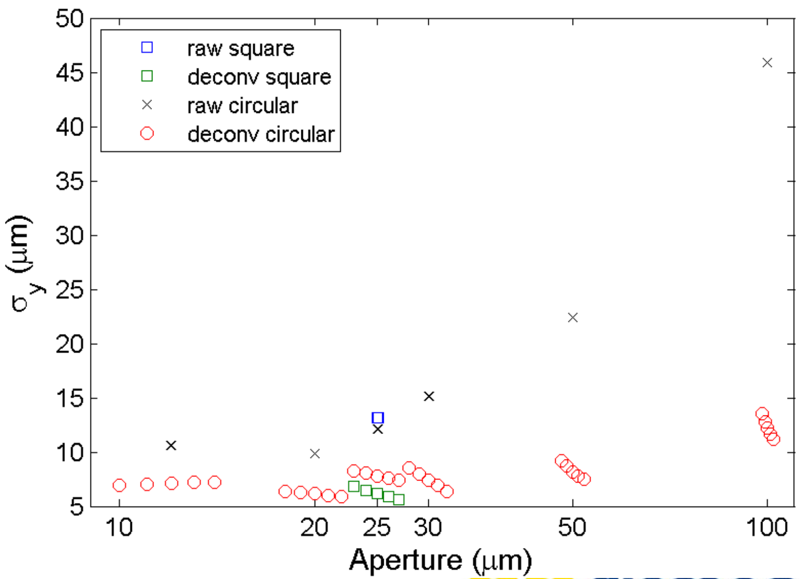

Deconvolved beam size with a range of defined apertures

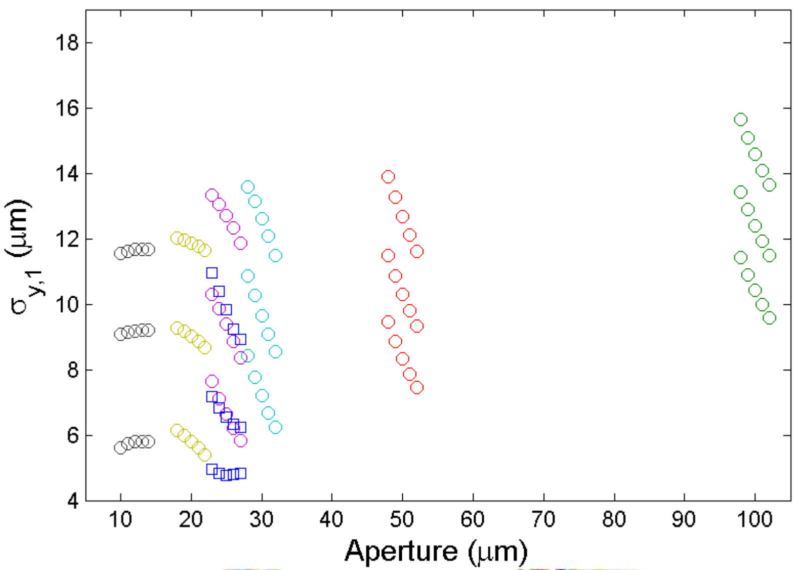

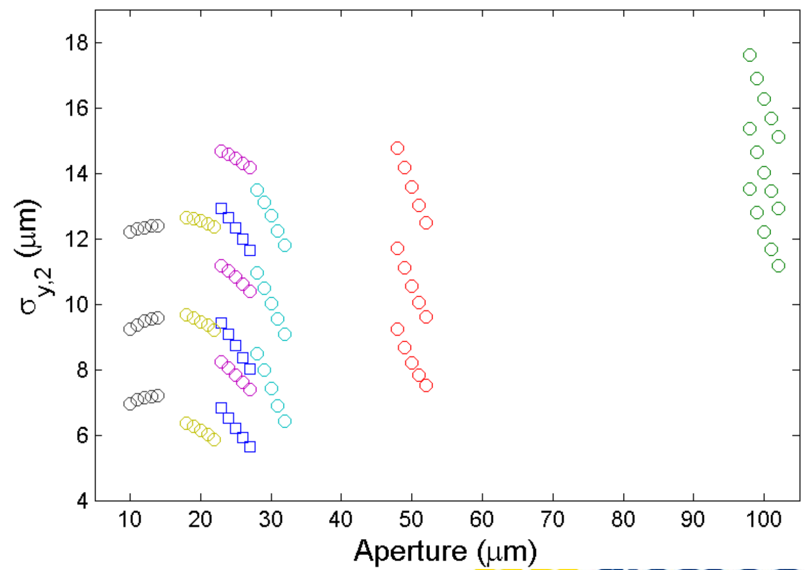

Deconvolved beam size with a range of defined apertures

- Vertical Emittance:
  - Twiss parameters at source position from LOCO by interpolation
  - Dispersion measured at the source

$$\varepsilon_y = (\sigma_y^2 - (\eta\ \sigma_\varepsilon)^2) / \beta$$

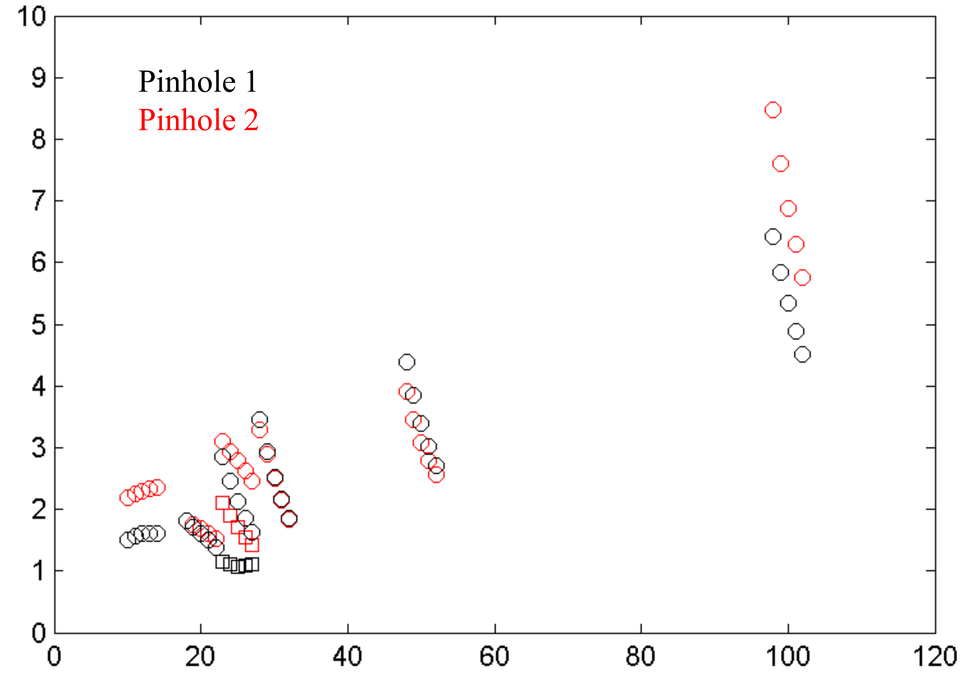

- Note:
  - if $\varepsilon_{x,y} \gg \lambda/2\pi$: Statistical Optics source description coincide with Geometrical Optics
    - This condition is necessary but not sufficient

- Condition sufficient:
  - $C = \max([2\pi\ \varepsilon\ \beta/(L_f\ \lambda)],1) \cdot \max([2\pi\ \varepsilon\ L_f\ /(\beta\ \lambda)],1) \gg 1$

- Lf for Bending Magnet: $L_f = \left(\frac{\lambda\rho}{2\pi}\right)^{\frac{1}{3}}$

  - for Diamond BM: C

ε_y (pm.rad)	λ=500nm	λ=40pm
10	1	$88 \,.\, 10^3$
1	1	$8.8 \,.\, 10^3$

diamond

Kinoform lenses

• Experimental results

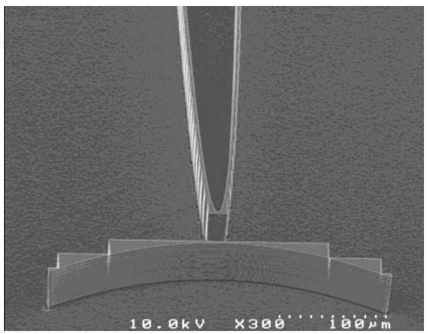

Focal length = 150 mm
Aperture & lens height = 280 um x 60 um
Focused beam size: 225 nm fwhm

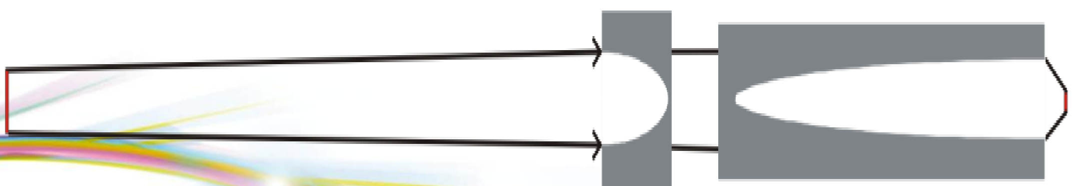

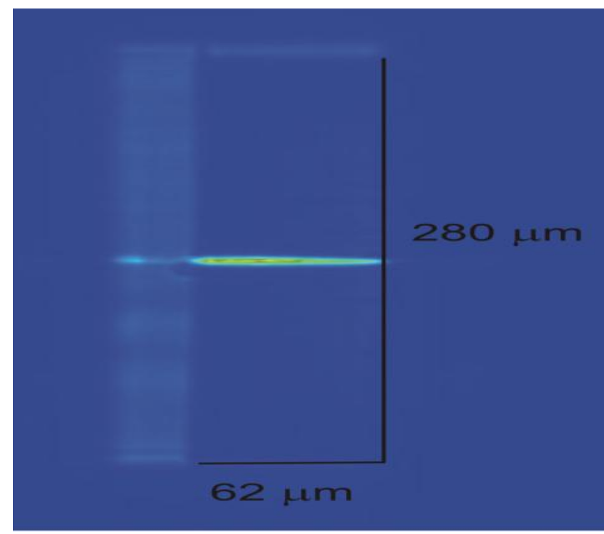

- Lucia Alianelli et al, *J. Synchrotron Rad.* **16** 325 (2009)
- Manoj Tiwari et al, *J. Synchrotron Rad.* **17** 237 (2010)
- Lucia Alianelli et al, *J. of Applied Physics* **108** 123107 (2010)
- Lucia Alianelli et al, *Optics Express* ***19*** *11120* (2011)

Courtesy from L. Alianelli

RayTracing used to simulate Coded Aperture

Courtesy of A. Haboub

To deal with magnification and Field of view issues

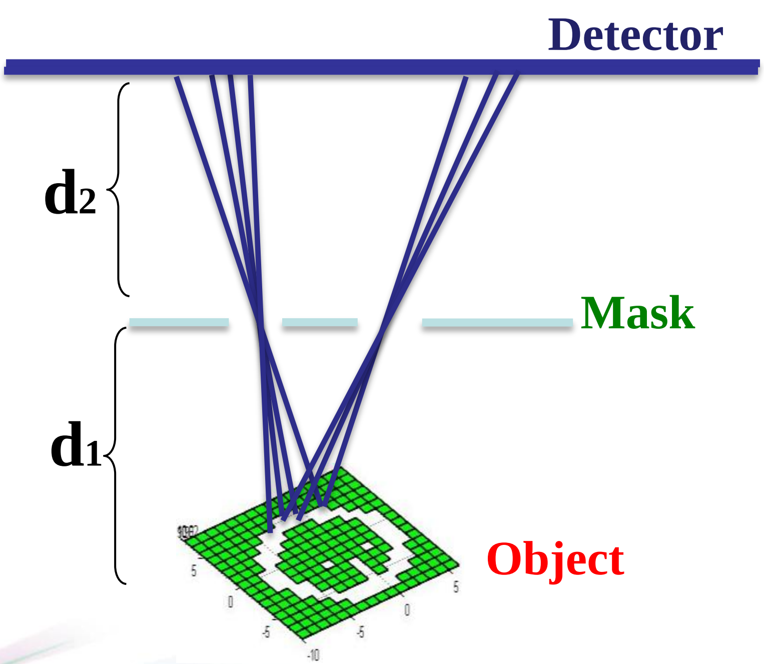

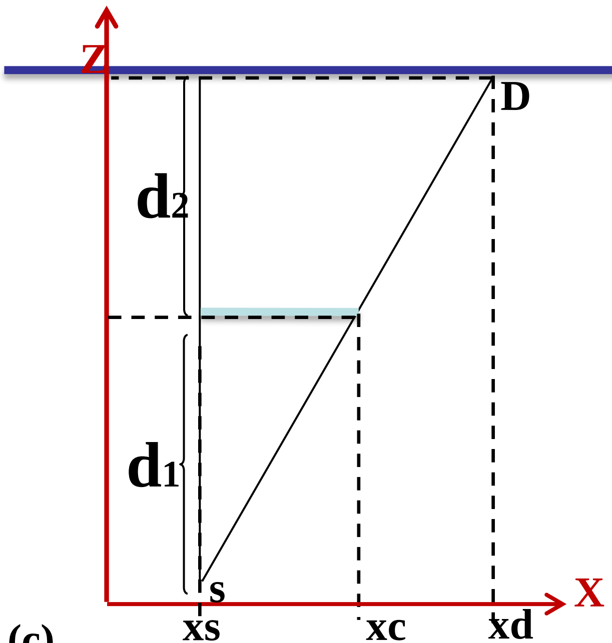

(a)

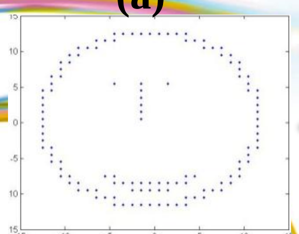

Plot of the object coordinates

(b)

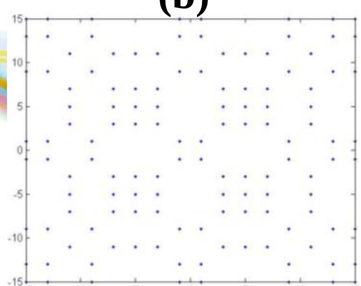

Plot of the mask coordinates

(c)

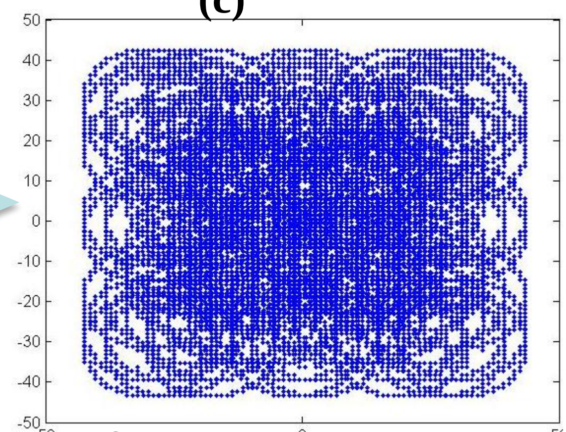

Plot of coded image coordinates

- Coded Apertures:
  - grids, gratings, or other patterns of materials opaque to various wavelengths of light. By blocking and unblocking light in a known pattern, a coded "shadow" is cast upon a plane of detectors.
    - Using computer algorithms, properties of the original light source can be deduced from the shadow on the detectors.
  - Examples of coded apertures:
    - Uniformly Redundant Array (URA)
    - Optimized RAndom pattern (ORA)
    - Hexagonal URA (HURA)
    - Modified Uniformly Redundant Array (MURA)
    - Fresnel Zone Plate (FZP)
    - ...

- URA, MURA, HURA, etc.

all URAs are related by the fact that they can be constructed from pseudo-noise (PN) sequences. (A PN sequence is a special type of binary sequence with a two-valued periodic autocorrelation function

Definition of an URA (Fenimore *et al.,* APPLIED OPTICS, **17**-3, p.337)

A is a $r \times s$ array with r,s prime numbers and $r - s = 2$

$$A(i,j) = \begin{cases} 0, & \text{if } i = 0 \\ 1, & \text{if } j = 0, i \neq 0 \\ 1, & \text{if } Q_r(i)Q_r(j) = 1 \end{cases}$$

where the quadratric residue Q_r is:

$$Q_r(p) = \begin{cases} 1, & \text{if there exists an integer x}, 1 \leq x < r \\ & \text{such that } p = mod_r\left(x^2\right) \\ -1, & \text{otherwise} \end{cases}$$

Coded Apertures

- URA, MURA, HURA, ORA, etc.

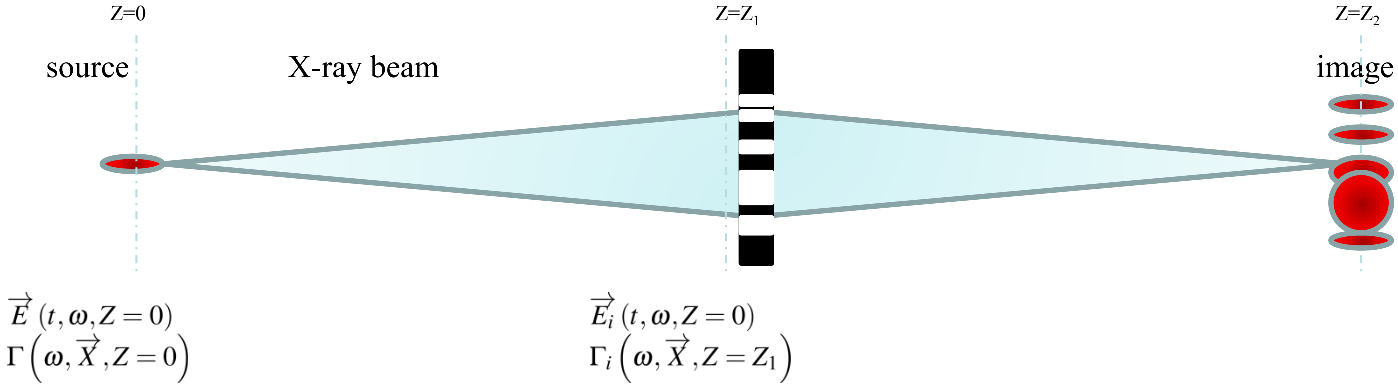

$$I(x,y) = S(x,y) \otimes A(x,y) + N(x,y)$$

Shot resolution estimation

- Want to know, what is the chance that a beam of a certain size is misfit as one of a different size?
- Tend to be photon statistics limited. (Thus coded aperture.)
- So:
  - Calculate simulated detector images for beams of different sizes
  - "Fit" images pairwise against each other:
    - One image represents true beam size, one the measured beam size
    - Calculate χ^2/ν residuals differences between images:

N = # pixels/channels
n = # fit parameters (=1, normalization)
S_i = expected number of photons in channel i

$$\frac{\chi^2}{\upsilon} = \frac{1}{N-n-1}\sum_{i=1}^{N}\frac{[s_i' - s_i]^2}{\sigma_i^2},$$

    - Weighting function for channel i: $\sigma_i = \sqrt{s_i}.$

  - Value of χ^2/ν that corresponds to a confidence interval of 68% is chosen to represent the 1-s confidence interval

diamond

Coded Aperture tests at ATF2

Data

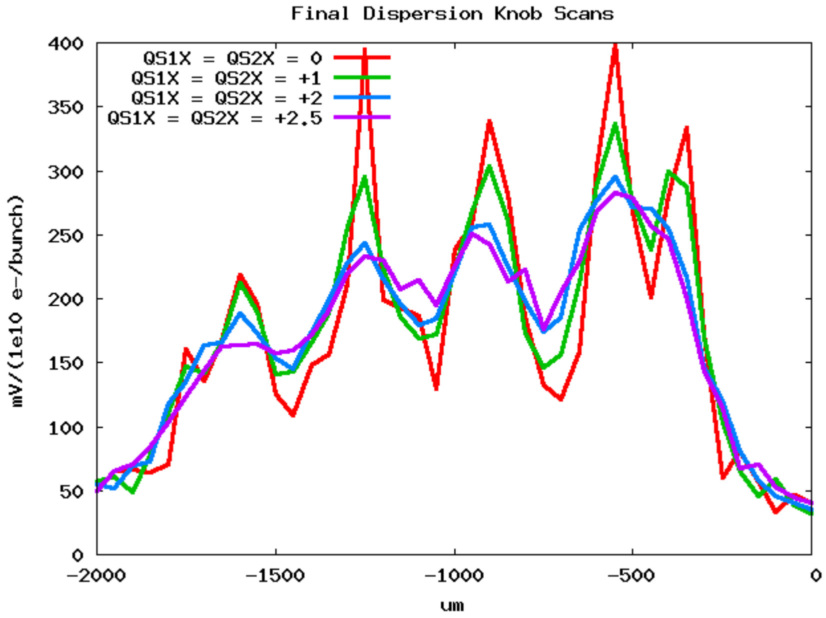

Simulations

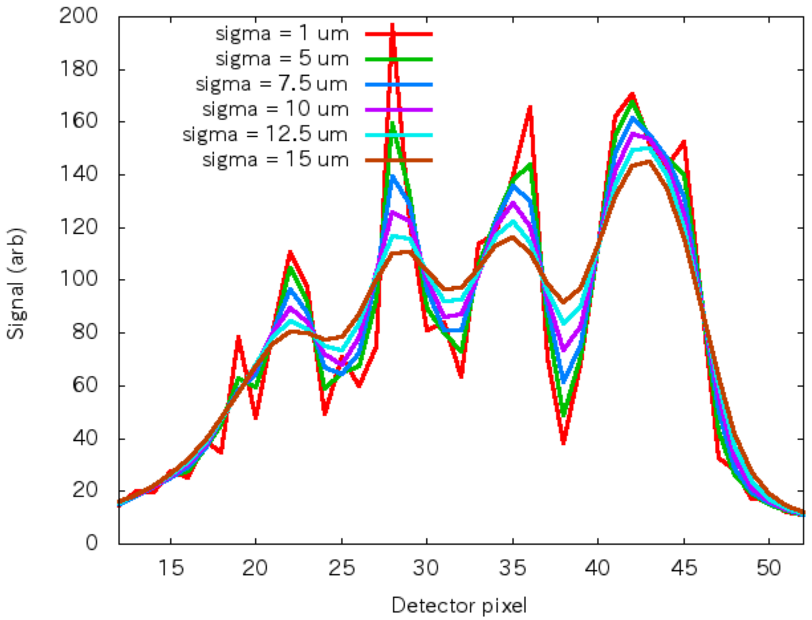

Used dispersion knob to change beam size

→Measured beams of 7.5 um or less with scanned-pixel (not single-shot) measurements

Why URA mask?

- Advantage over simple pinhole/slit:
  - Greater open aperture for single-shot measurements
  - Somewhat better resolution
    - Get some peak-valley ratios that help at smaller beam sizes.
    - Make use of more of the detector
- What about a simple equal-spaced array of pinholes/slits?
  - Flatter spatial frequency response
    - Better chance of reconstructing shape
    - Unique position determination (non-repeating pattern)
  - On the other hand, an equal-spaced array can offer tuned resolution over a narrower range of sizes
    - Array may be suitable for a very stable machine, such as a light source.
- For instability studies (e-cloud, e.g.) or other machine studies, or for a luminosity machine which is always running at the limit of stability, a URA mask promises reasonable performance over a range of bunch conditions.
- However, depending on the beam characteristics and measurements desired, URA is not necessarily the optimal pattern for a given measurement problem.
  - Other coded aperture patterns also currently under investigation

Concept of Coded Aperture Imaging

Courtesy of A. Haboub

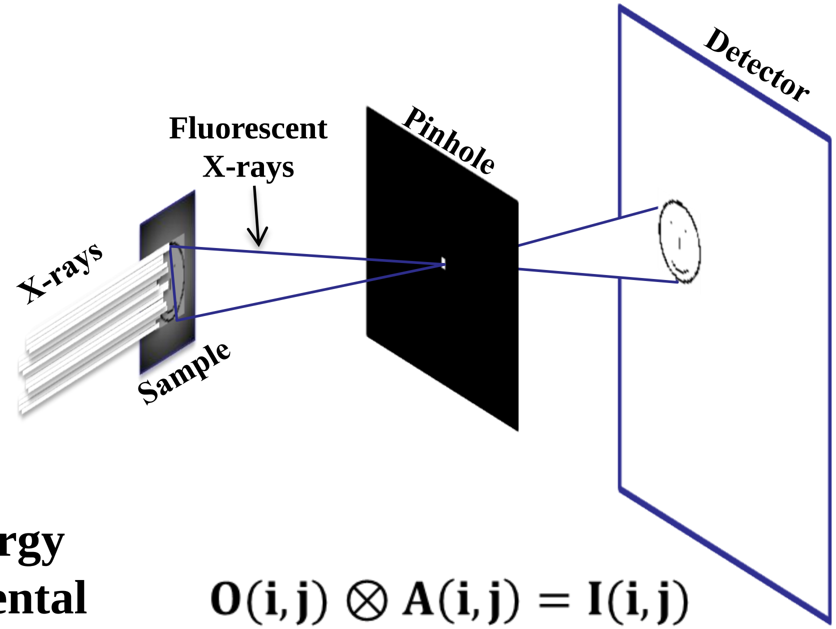

$$\mathbf{O(i,j) \otimes A(i,j) = I(i,j)}$$

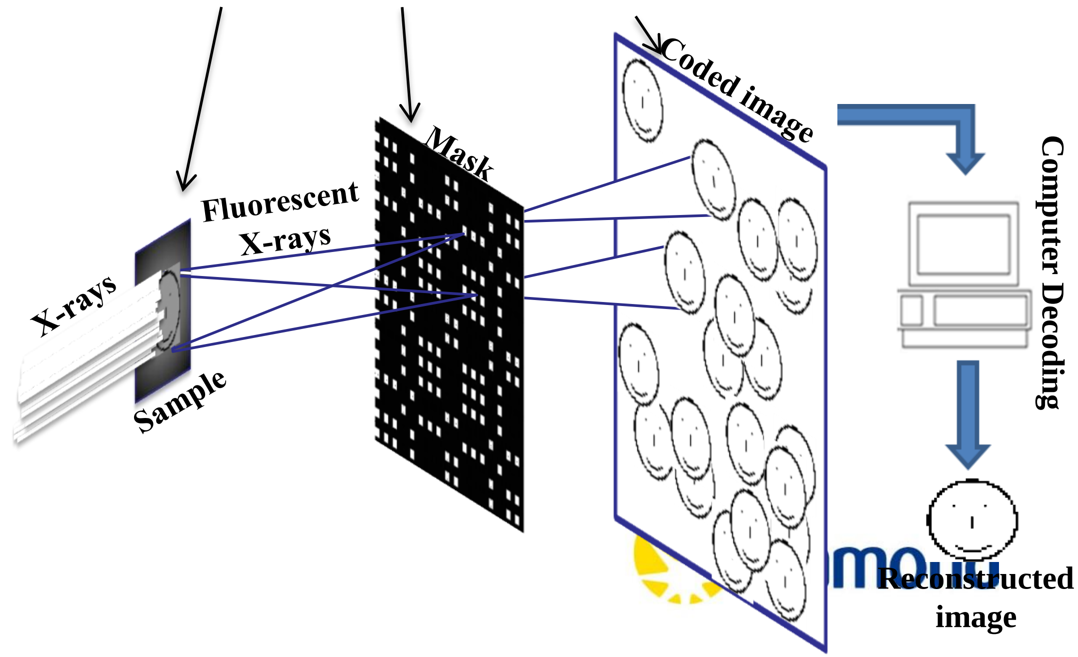

- **Coded aperture imaging allow lensless imaging at high photon energies and larger FOVs.**
- **Coded aperture imaging with fluorescent x-ray source, and an energy resolving CCD can yield to 3D elemental map of the sample.**
- **The detector response is**

$$\mathbf{I(i,j) = O(i,j) \otimes A(i,j)} \qquad \mathbf{(1)}$$

- **Image reconstruction through post-processing**

$$\mathbf{O'(i,j) = I(i,j) \otimes \tilde{A}(i,j)} \qquad \mathbf{(2)}$$

$$\mathbf{A(i,j) \otimes \tilde{A}(i,j) = \delta} \qquad \mathbf{(3)}$$

Magnification >1

Kinoform lenses

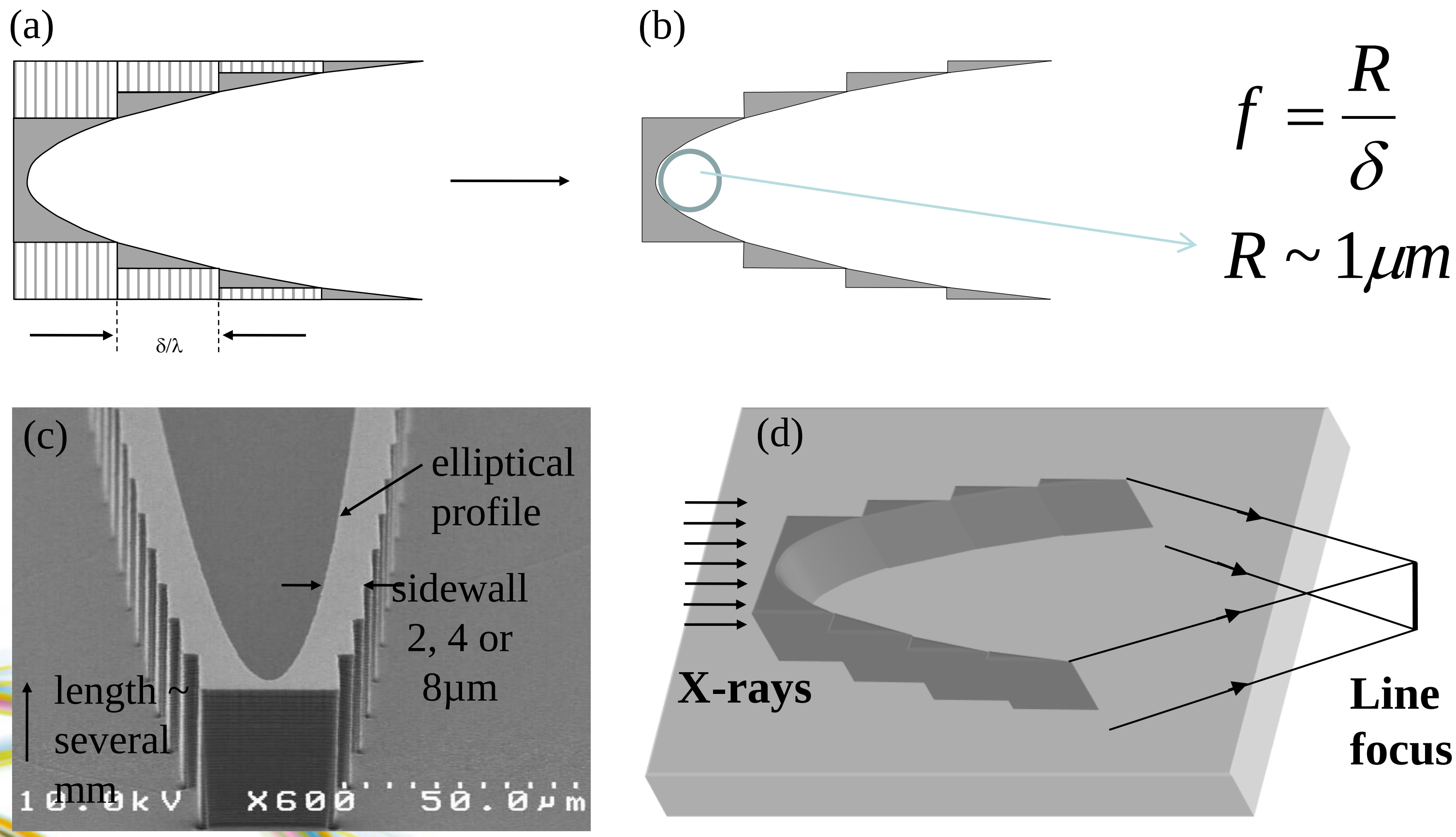

Schematic of a kinoform lens before (a) and after removal of redundant 2π phase-shifting material (b). **SEM micrograph of a Si kinoform lens depicting important parameters (c)**. Focusing action of a kinoform lens (d).

diamond

Courtesy from L. Alianelli

Courtesy of Dr. J. Vila-Comamala

Au FZP for 8-12 keV photon energy

FZPs for sub 100-nm focusing

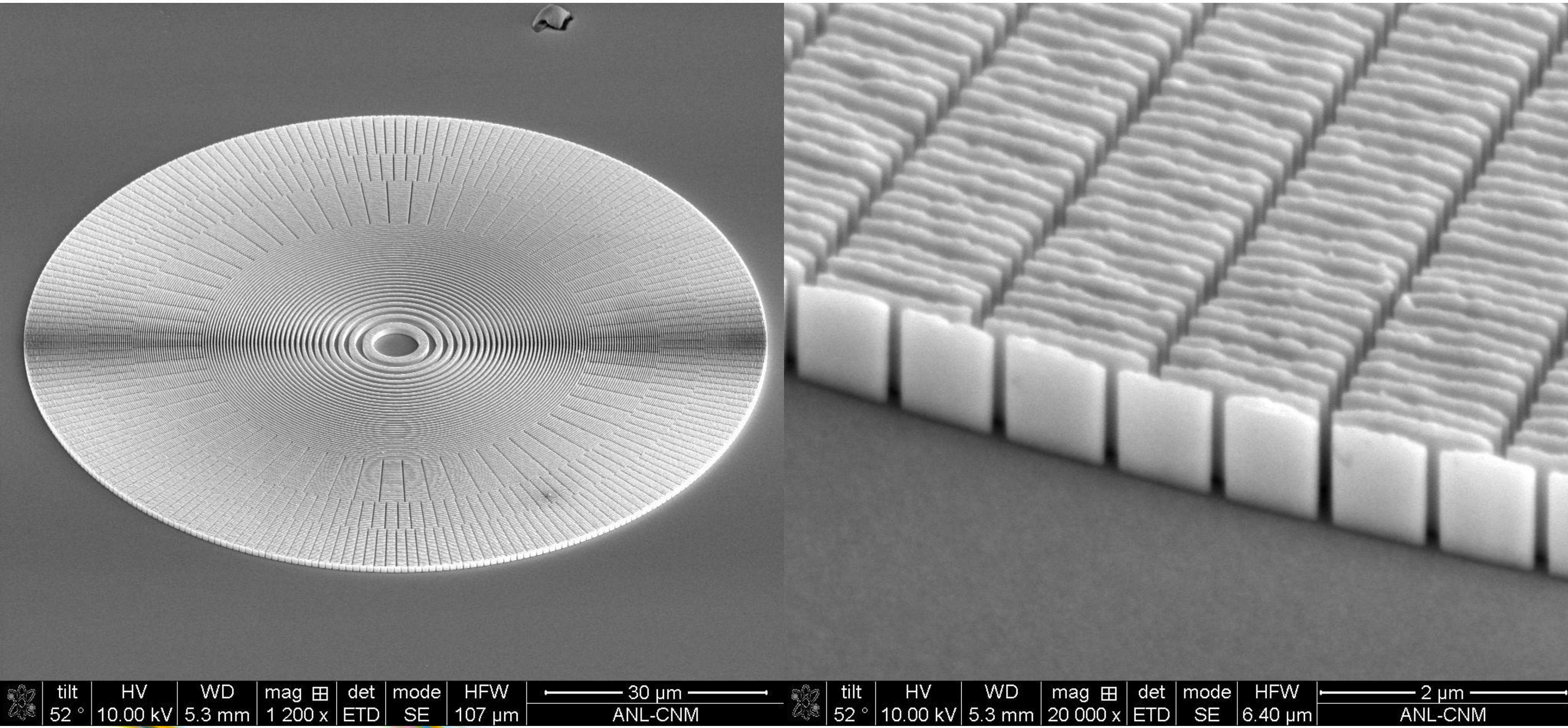

Au FZP, D = 100 um, dr = 100 nm, t ~ 900 nm

Courtesy of Dr. J. Vila-Comamala

Au FZP for 8-12 keV photon energy

FZPs for sub 100-nm focusing

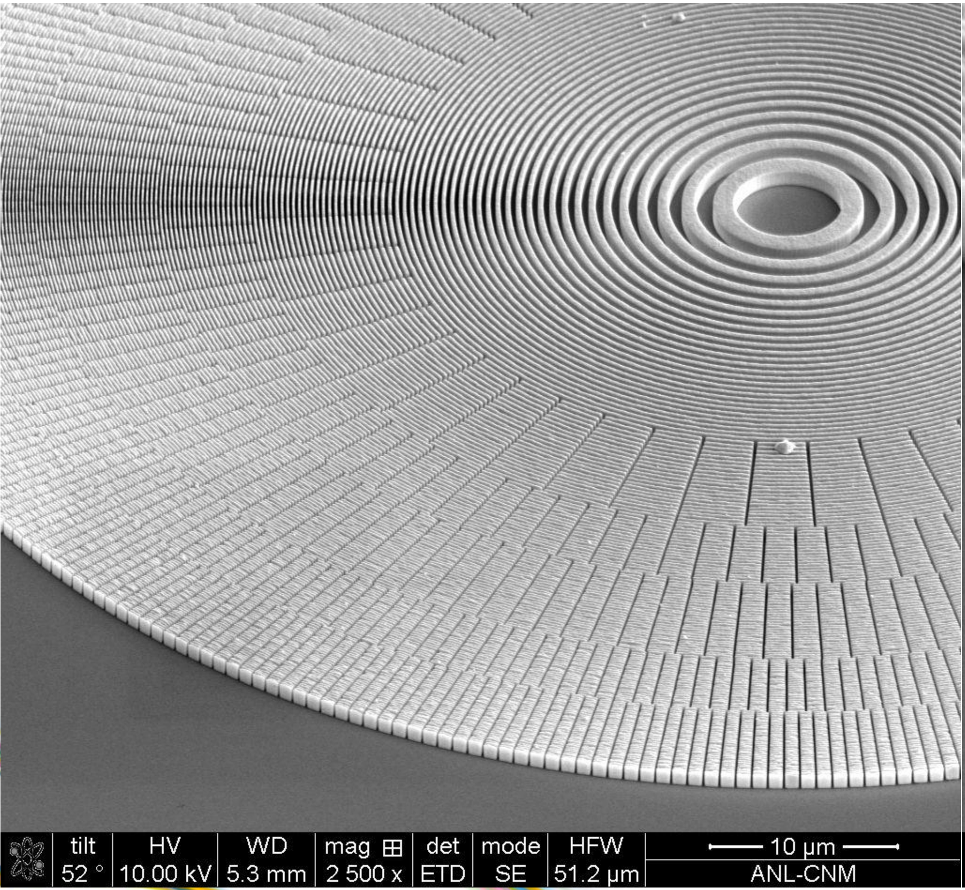

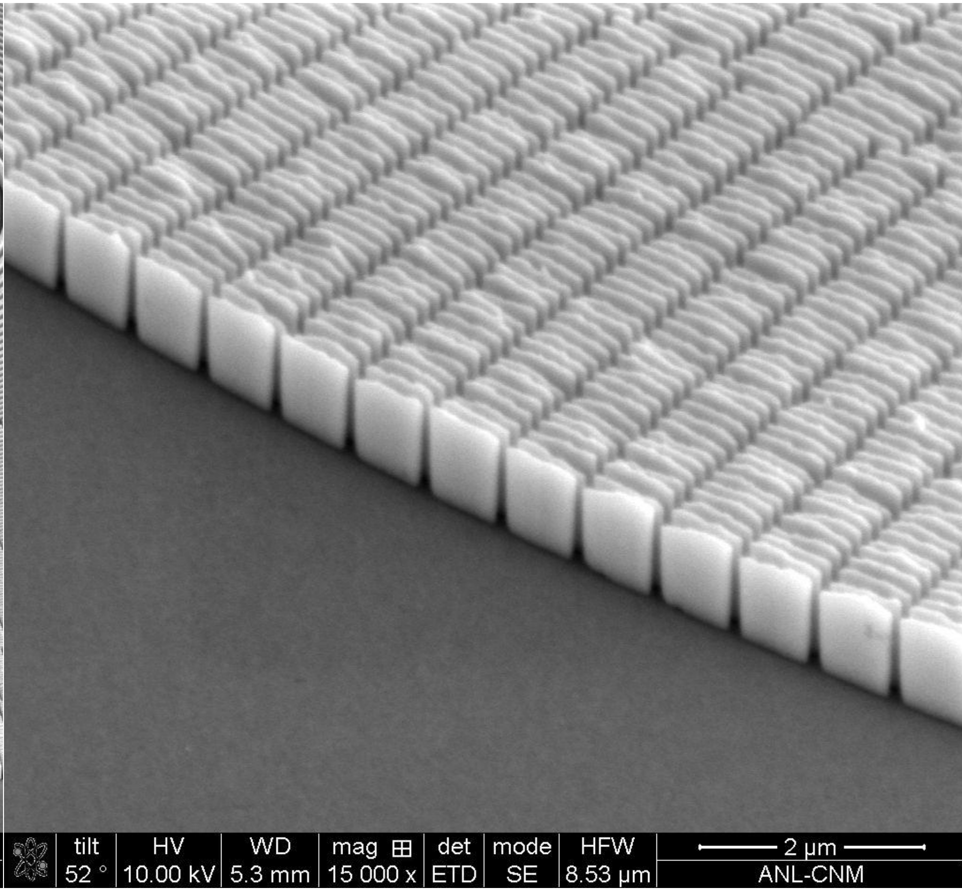

Au FZP, D = 100 um, dr = 80 nm, t ~ 900 nm

diamond

Courtesy of Dr. J. Vila-Comamala

Au FZP for 8-12 keV photon energy

FZPs for sub 100-nm focusing

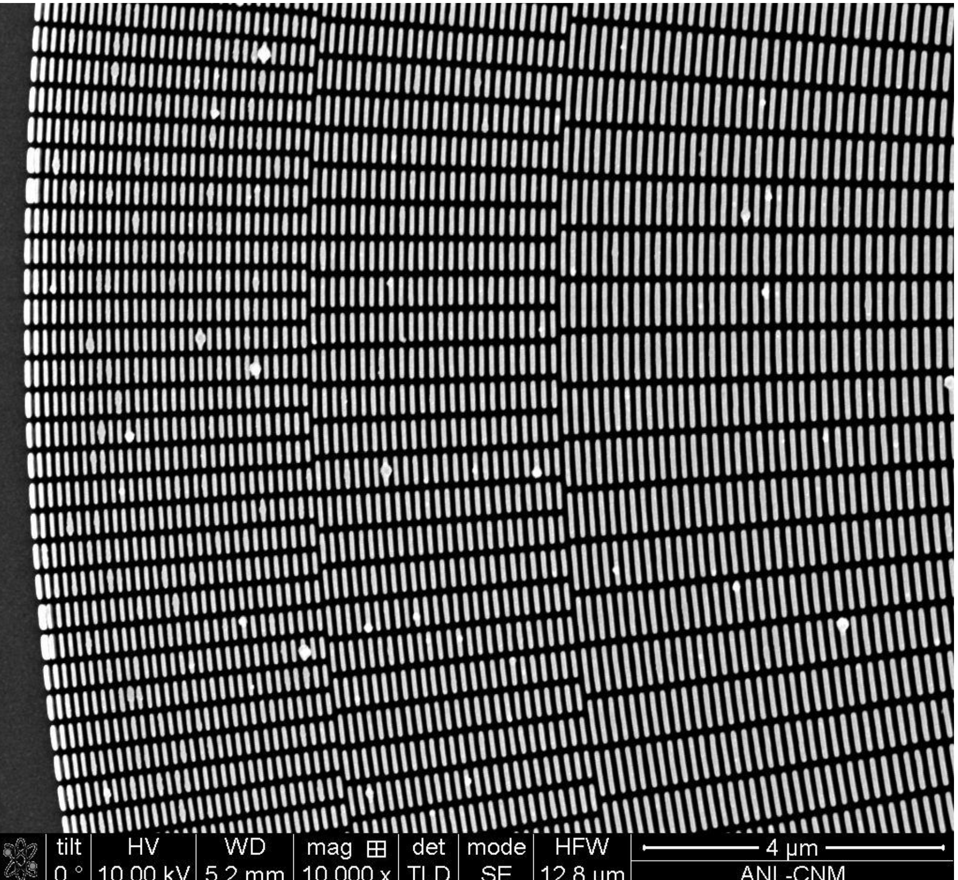

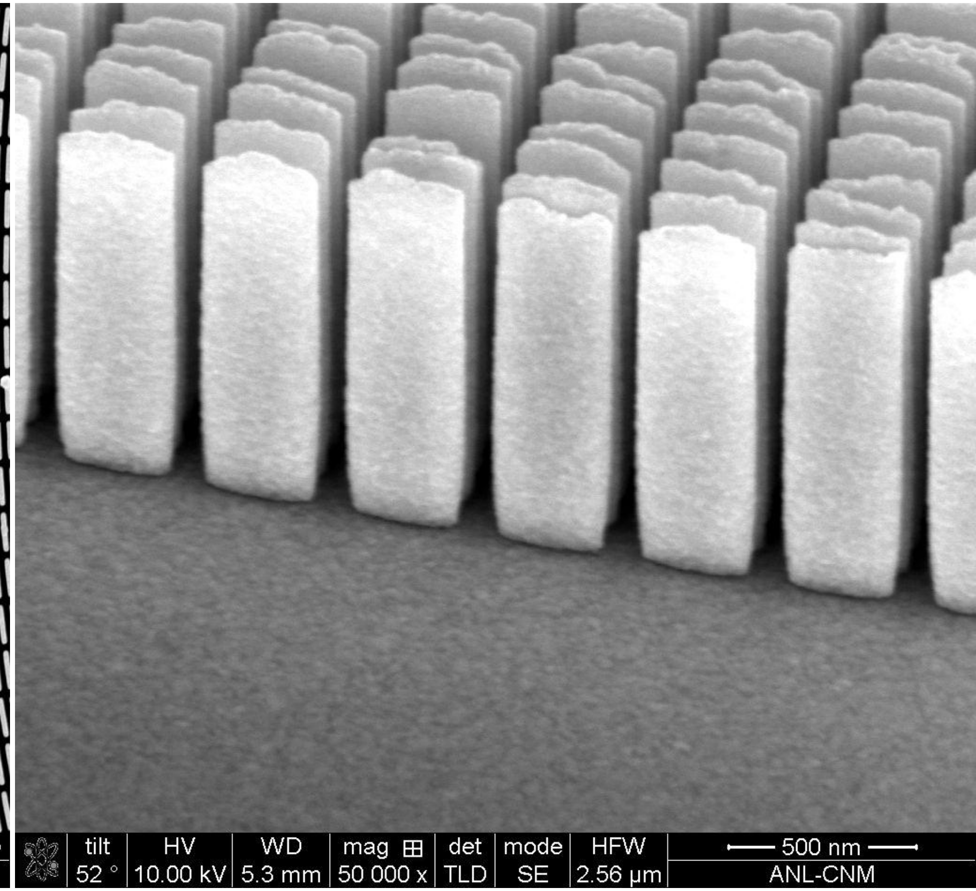

Au FZP, D = 100 um, dr = 60 nm, t ~ 1100 nm

Courtesy of Dr. J. Vila-Comamala

Ir-HSQ Fresnel Zone Plates for Hard X-rays made at PSI (6—10 keV)

Diameter, D = 150 and 100 μm

Outermost zone width, dr = 20

Zone thickness, t ~ 500—600 nm

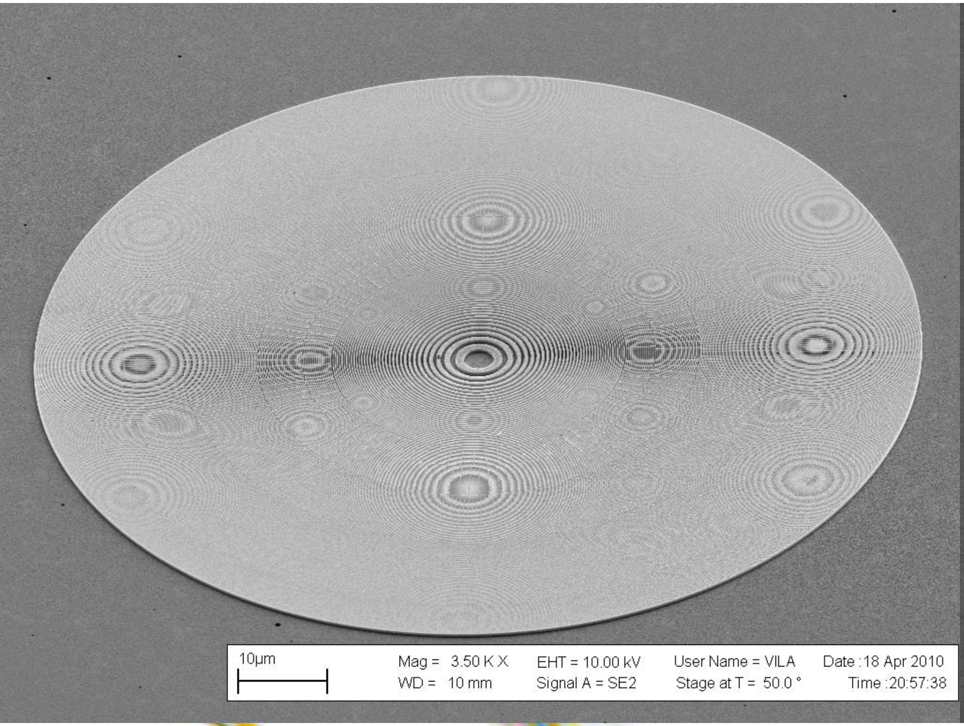

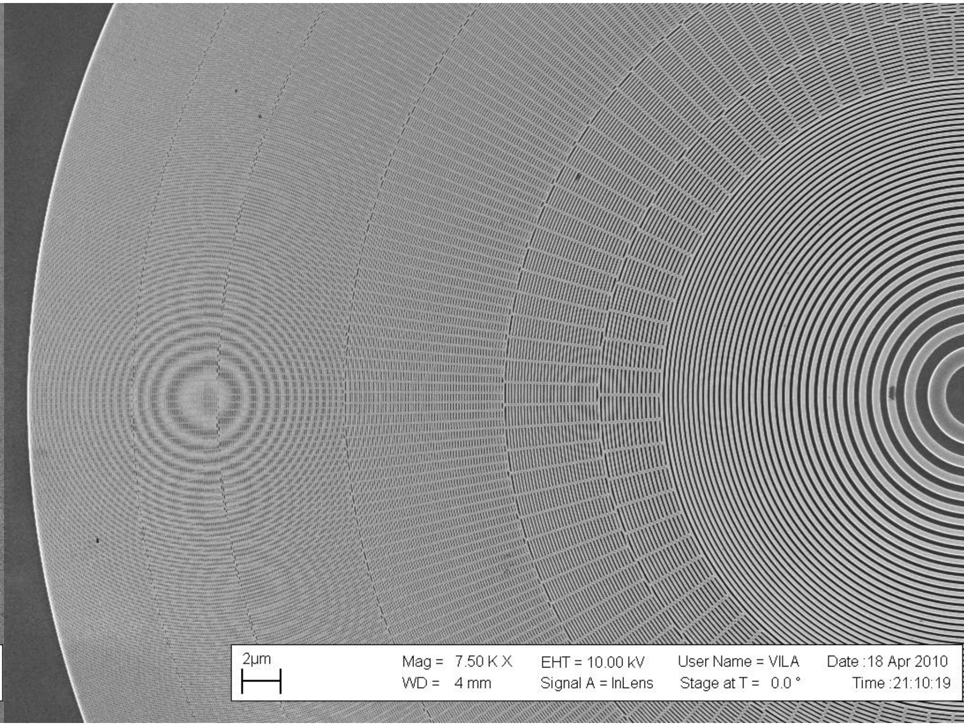

J. Vila-Comamala et al., Nanotechnology (2010)

J. Vila-Comamala et al., Optics Express (2011)

diamond

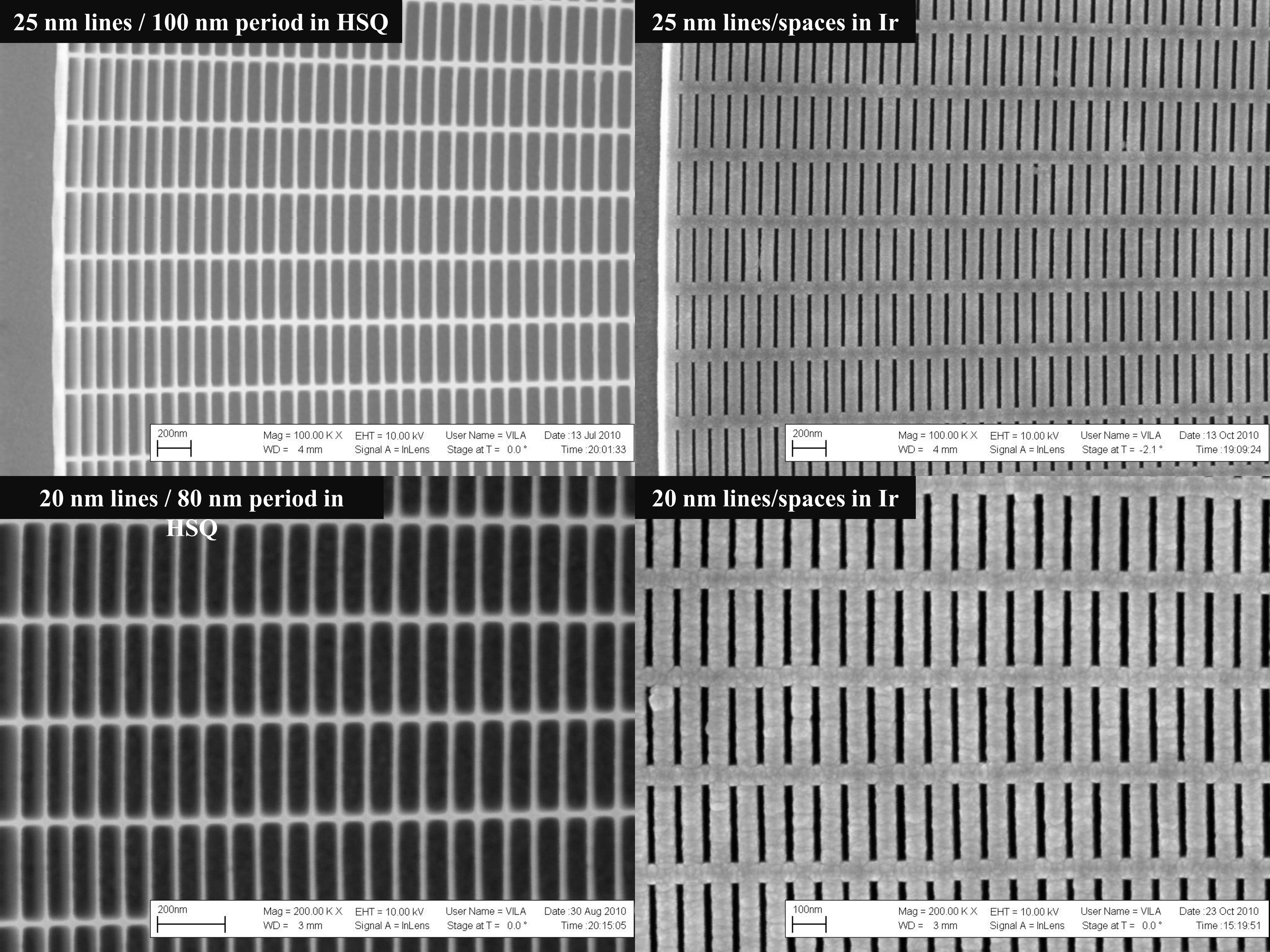
25 nm lines / 100 nm period in HSQ
200nm
Mag = 100.00 K X
WD = 4 mm
EHT = 10.00 kV
Signal A = InLens
User Name = VILA
Stage at T = 0.0 °
Date :13 Jul 2010
Time :20:01:33
25 nm lines/spaces in Ir
200nm
Mag = 100.00 K X
WD = 4 mm
EHT = 10.00 kV
Signal A = InLens
User Name = VILA
Stage at T = -2.1 °
Date :13 Oct 2010
Time :19:09:24
20 nm lines / 80 nm period in HSQ
200nm
Mag = 200.00 K X
WD = 3 mm
EHT = 10.00 kV
Signal A = InLens
User Name = VILA
Stage at T = 0.0 °
Date :30 Aug 2010
Time :20:15:05
20 nm lines/spaces in Ir
100nm
Mag = 200.00 K X
WD = 3 mm
EHT = 10.00 kV
Signal A = InLens
User Name = VILA
Stage at T = 0.0 °
Date :23 Oct 2010
Time :15:19:51